Newsletters on Stratigraphy, Vol. 58/1 (2025), 99–123
Published online February 25, 2025; published in print March 2025

The early depositional history of the Pisco Formation (Middle to Upper Miocene, Peru)

Elisa Malinverno[1,*], Giulia Bosio[2], Maria Elena Gastaldello[1], Luca Pellegrino[3], Giovanni Bianucci[2], Alberto Collareta[2], Karen Gariboldi[2], Mario Urbina[4], Igor M. Villa[1] and Claudio Di Celma[5]

With 11 figures

Abstract. The East Pisco Basin of Peru is a world-renowned Fossil-Lagerstätte that has yielded an abundant and exceptionally well-preserved record of marine vertebrates within a sedimentary succession ranging in age from the middle Eocene to, at least, the Late Miocene. Owing to its remarkable wealth of fossil discoveries, the Miocene Pisco Formation is the most famous unit in the basin. Its stratigraphic architecture has been recently redefined in the Ica River Valley, with the identification of three depositional sequences (P0, P1 and P2, in ascending order), separated by extensive unconformities that testify to periods of subaerial exposure correlated with major climatic cycles.

While P1 and P2 provided abundant diatom markers and several volcanic ash layers dated through the $^{40}Ar/^{39}Ar$ method (P1, 9.5–8.6 Ma; P2, 8.4–6.7 Ma), the exposures of P0 that defined this unit were found to be barren of microfossils and lacked ash layers, thus their dating relied solely on strontium isotope stratigraphy (14.7–12.6 Ma). Here, we analyze a new section including P0 and P1 at Cerro Tiza. It represents a deeper portion of the Miocene Pisco Basin in the Ica River Valley, and features abundant siliceous markers, allowing for a good biostratigraphic control of the early Pisco deposits. Notably, the biostratigraphic age assignment of P0 in this work (14.2–12.9 Ma) confirms previous age estimates obtained through the strontium-isotope ratio and allows a chronological correlation with the Laberinto, Pampa and Naranja members of the Pisco Formation in the Laberinto area. Furthermore, stratigraphic markers and one ash layer from the P1 sequence indicate that deposition of this unit started earlier than hitherto recognized (slightly before 10 My), thus shortening the extension of the stratigraphic gap separating the two sequences. The microfossil assemblages also allowed for better constraining the paleoclimatic and paleoceanographic conditions that characterized the early depositional phases of the Pisco Formation.

Keywords. Pisco Basin; diatoms; silicoflagellates; tephra

Authors' addresses:
[1] Dipartimento di Scienze dell'Ambiente e della Terra, Universita degli Studi di Milano-Bicocca, Piazza della Scienza 4, 20126 Milano, Italy
[2] Dipartimento di Scienze della Terra, Università di Pisa, Via S. Maria 53, 56126 Pisa, Italy
[3] Dipartimento di Scienze della Terra, Università degli Studi di Torino Via Valperga Caluso, 35, 10125 Torino, Italy
[4] Departamento de Paleontología de Vertebrados, Museo de Historia Natural, Universidad Nacional Mayor de San Marcos, Lima 1, Peru
[5] Scuola di Scienze e Tecnologie, Università degli Studi di Camerino, Via Gentile III da Varano 7, 62032 Camerino, Italy
* Corresponding author: elisa.malinverno@unimib.it

DOI: 10.1127/nos/2025/0864 Borntrager Science Publishers, Stuttgart, www.borntraeger-cramer.de

1 Introduction

The Pisco Formation, widely exposed in the Ica River Valley and renowned for its significant fossil vertebrate record (e.g., Lambert et al. 2010, Esperante et al. 2015, Gariboldi et al. 2015, Gioncada et al. 2016, Bosio et al. 2021, Collareta et al. 2021b), is composed of at least three depositional sequences that reflect the interplay between tectonics and eustasy (Di Celma et al. 2017, 2018a). These sequences were defined on the western side of the Ica River valley, in an area stretching some 22 km between Cerro Blanco (close to the village of Ocucaje) to the north, and Cerro las Tres Piramides (next to the broad Zamaca area) to the south, where an almost uninterrupted exposure of the Pisco Formation strata is available (Di Celma et al. 2017).

Each of these sequences, named P0, P1 and P2 in ascending order (Di Celma et al. 2017, 2022) and separated by basin-wide unconformities, is characterized by a diverse and specific vertebrate fossil content (Bianucci et al. 2016, Bianucci & Collareta 2022) that provides exceptional evidence of the evolutionary history of marine vertebrates (i.e., Bianucci et al. 2024). As such, in order to document the temporal distribution pattern of the marine vertebrate faunas, it is paramount to accurately date each sequence with the highest possible accuracy.

Detailed biostratigraphic and tephrochronologic analyses along measured stratigraphic sections across the Ica River Valley allowed the age interval of P2 (8.4–6.7 Ma) and P1 (9.5–8.6 Ma) to be constrained (Gariboldi et al. 2017, Bosio et al. 2019, 2020a,c), even if an older age was inferred for the base of P1 (DeVries & Jud 2018). The age of P0, that was sand-grained, lithogenic in composition, barren of microfossils and lacked tephra layers, was previously estimated based on the age of underlying and overlying strata; more recent analyses through strontium isotopes on shark teeth, oysters and barnacles, resulted in a well-defined chronostratigraphic assessment of its duration (14.7–12.6 Ma) (Bosio et al. 2020b, 2022).

Recent work by DeVries et al. (2021) correlated the Pampa and Naranja members of the Pisco Formation, exposed in the Laberinto area (Fig. 1), with the P0 sequence of the Ica River Valley and dated these three members between 14.4 and 12.8 Ma by diatoms from different sediment samples.

Here, we provide new biostratigraphic data and a paleoecological constraint from a new find of P0 and an extended section of P1, exposed on the eastern and southern flank of Cerro Tiza (Fig. 1), a locality at the SW margin of the Ica River Valley (Di Celma et al. 2022). This succession represents a basinward portion of the basin fill, displaying the most continuous and expanded successions documented so far for this unit.

2 Geological setting

The Pisco Basin is a forearc basin, elongated along the Peru trench, that formed as a consequence of the subduction of the Nazca Plate underneath the South American Plate (Thornburg & Kulm 1981, Kulm et al. 1982). The Pisco Basin is subdivided by the Outer Shelf High – Coastal Cordillera structural high (Romero et al. 2013) into an offshore submerged West Pisco Basin and an onshore East Pisco Basin, which is today mostly exposed on land (Fig. 1A). These forearc basins underwent a complex history of subsidence and uplift (von Huene & Suess 1988, Herbozo et al. 2020, Viveen & Schlunegger 2018) that is documented by their sedimentary fill and stratigraphic gaps.

The stratigraphic succession of the East Pisco Basin is formed by two tectonostratigraphic packages, namely the P and N megasequences, lying on the basement and separated by a basin-wide unconformity, characterized by a prolonged interval of erosion/non-deposition (Di Celma et al. 2022). The P megasequence begins with the Paracas Formation, displaying a basal coarse-grained layer, rich in benthic foraminifera, followed by a calcareous silt with abundant calcareous nannofossils, referred to the middle Eocene (~43.6–37.4 Ma) (Coletti et al. 2019, Malinverno et al. 2021). It is followed by the Otuma Formation, characterized by a basal sandstone of variable thickness containing frequent mollusks (DeVries 1998, DeVries et al. 2017) and an overlying siltstone containing calcareous nannofossils in the basal part and diatomaceous

Fig. 1. Geological framework. A) Aerial view of the East Pisco Basin with the position of the main localities (from Google Earth satellite imagery); inset: location of the East Pisco Basin in the Ica Region; B) Geological map of the western side of the Ica River Valley (redrawn and modified from Di Celma et al. 2022); C) detailed geological map of the area of Cerro Tiza and location of the sampled sections.

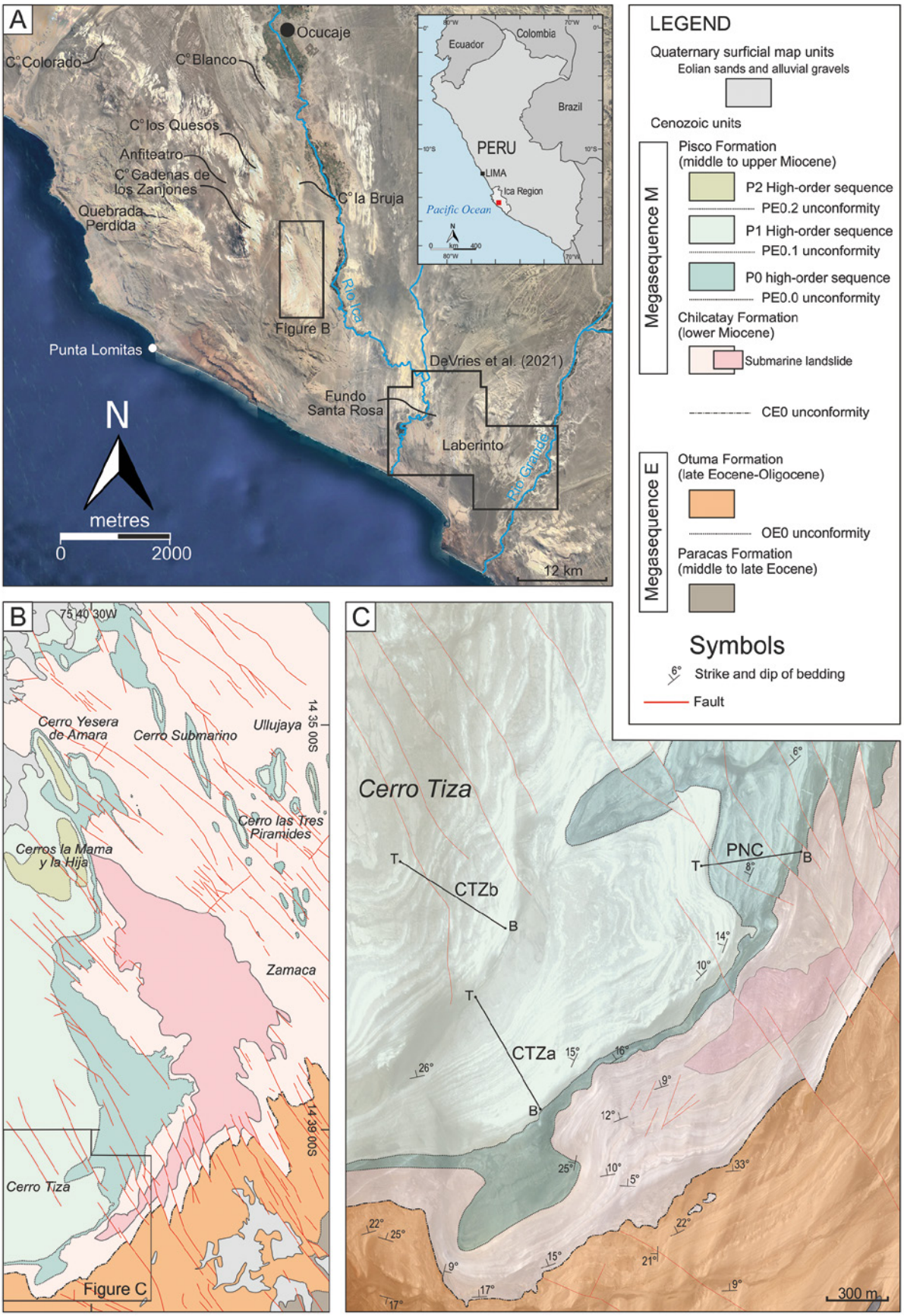
A
Ocucaje
C° Colorado
C° Blanco
C° los Quesos
Anfiteatro
C° Cadenas de los Zanjones
Quebrada Perdida
C° la Bruja
Río Ica
Figure B
Punta Lomitas
DeVries et al. (2021)
Fundo Santa Rosa
Laberinto
Río Grande
N
metres
0
2000
12 km
Ecuador
Colombia
Brazil
PERU
LIMA
Ica Region
Pacific Ocean
LEGEND
Quaternary surficial map units
Eolian sands and alluvial gravels
Cenozoic units
Megasequence M
Pisco Formation
(middle to upper Miocene)
P2 High-order sequence
PE0.2 unconformity
P1 High-order sequence
PE0.1 unconformity
P0 high-order sequence
PE0.0 unconformity
Chilcatay Formation
(lower Miocene)
Submarine landslide
CE0 unconformity
Megasequence E
Otuma Formation
(late Eocene-Oligocene)
OE0 unconformity
Paracas Formation
(middle to late Eocene)
Symbols
Strike and dip of bedding
Fault
B
75°40'30"W
14°35'00"S
Cerro Yesera de Amara
Cerro Submarino
Ullujaya
Cerro las Tres Piramides
Cerros la Mama y la Hija
Zamaca
14°39'00"S
Cerro Tiza
Figure C
C
Cerro Tiza
T
CTZb
B
PNC
CTZa
300 m

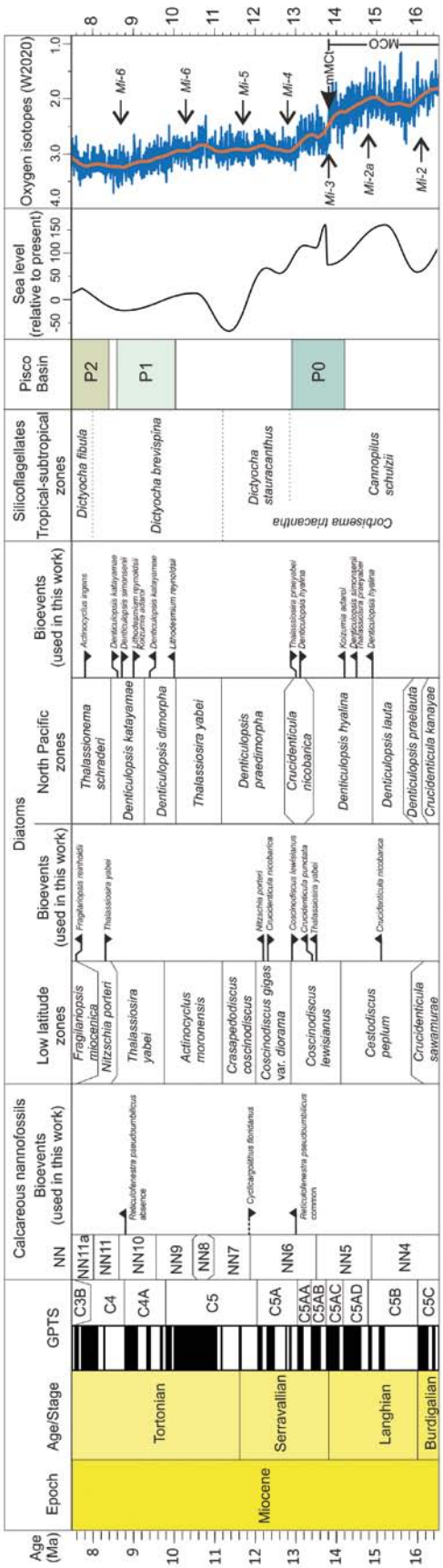

Fig. 2. Stratigraphic framework for the Middle-early Late Miocene interval of the Pisco Formation, plotted using Time Scale Creator calibrated with the GTS2020 (Gradstein et al. 2020) and modified in Corel Draw. **Calcareous nannofossils:** Martini (NN) zones: revised ages are from low and middle latitudes zonation of Backman et al. (2012) and calibrated to the GTS2020. **Diatoms: Low-Latitude zones** are from Barron (2015; 2006 – Site 1219) and Scherer et al. (2007); main age calibration and other events/zones are revised using Raffi et al. GTS2020 (Table 29.6); additional Neogene events from earlier Barron-Baldauf papers used in GTS2012 version. **N Pacific zones** are from Scherer-Gladenkov-Barron (2007) update of Neogene diatoms of Maruyama & Shiono 2003. Bioevents from both areas used in this work are plotted, following the BDC. **Silicoflagellate** zones are from Bukry, 1981, modified by Perch-Nielsen, 1985, linked to NN biozones. Sea-level curve: offsets from long-term curve from Hardenbol et al. (SEPM charts, 1998). **Benthic oxygen isotope curve** plottedfrom Table S34 of Westerhold et al. (2020): blue, 25kyr smoothing, red: long-term trend. **Mi events** from Boulila et al. (2011) based on definitions by Miller et al. (1991, 1998) and additional calibrations by Pekar et al. (2002).

layers in the upper part. The base of the Otuma Formation has been constrained through biostratigraphic studies and absolute tephra dating to the late Eocene (~37 Ma) (DeVries 2019, Malinverno et al. 2021), and its top represents a latest Eocene age in most outcrops (Malinverno et al. 2021) with an early Oligocene age being documented at some locations (DeVries et al. 2017, 2021).

The N Megasequence starts with the Tunga Formation, a recently-defined ~80 m thick unit formed by basal sandstones followed by silty mudstones intercalated with fine sandstones that were deposited between 21.6 and 20.5 Ma, as dated by diatom biostratigraphy (DeVries et al. 2024). The Tunga Formation is unconformably overlain by the Chilcatay Formation, a dominantly coarse-grained unit formed by three high-order sequences, namely Ct0, dated to the early Early Miocene (~20–19.5 Ma, DeVries et al. 2024, but see also DeVries et al. 2021 and Bosio et al. 2022), Ct1 and Ct2, constrained to the late Early Miocene (19.2–18.0 Ma, Belia et al. 2018, Bianucci et al. 2018, Di Celma et al. 2018b, Lambert et al. 2018, Bosio et al. 2020a,b, 2022). Finally, the Pisco Formation is formed by three high-order sequences (Fig. 2): the sandy to silty P0, dated by Sr isotope stratigraphy to the Middle Miocene (between 14.7 and 12.6 Ma, Bosio et al.

2020b, 2022), and the diatomaceous P1 and P2 dated by diatom biostratigraphy and absolute dating on tephra layers to the Late Miocene (9.5–8.6 Ma, and 8.4 to ≥ 6.71 Ma, respectively, Gariboldi et al. 2017, Bosio et al. 2020a,c).

3 Materials and methods

3.1 Field work

A detailed mapping of the area of Cerro Tiza was carried out between 2021 and 2024, integrating the larger-scale geological map resulting from the 2014–2018 field campaigns (Fig. 1B), by walking out the PE0.0 and PE0.1 unconformities in the field with a GPS and virtually tracing them in Google Earth 2023 images (Fig. 1C). A composite stratigraphic section encompassing P0 and P1 was measured at 10 cm resolution and sampled continuously at ~1.5 m resolution (Fig. 3). Additional samples were collected in the surrounding area to complete the biostratigraphic assessment.

In particular, P0 was measured and sampled on the eastern flank of Cerro Tiza (PNC section, 14°39'28.40"S – 75°40'9.80"W), where a seemingly undisturbed succession, bounded by unconformities, crops out; additional samples were collected at different locations on the southern and south-eastern flank of the hill, following the unconformities (samples PNC24-D1-D5 and CTi-D15, D100). P1 was measured along two tracks on the southern flank of Cerro Tiza (CTZa-b sections, 14°40'10.10"S – 75°40'51.60"W).

The floral assemblages are compared with those from previously-measured sections at Cerro Cadenas de los Zanjones (ZANJ and LA section, 14°34'15.74"S – 75°43'44.21"W), Ullujaya (UL, 14°35'26.50"S – 75°38'44.00"W) and Cerros la Mama y la Hija (MF, 14°36'46.50"S – 75°40'27.00"W), whose stratigraphy was already assessed by Bosio et al. (2020a) (ZANJ and MF), Di Celma et al. (2018b) (UL) and Di Celma et al. (2019) (Zamaca area) as well as with those of the Laberinto area of DeVries et al. (2021).

3.2 Microfossils

Samples for microfossil analyses were prepared as standard smear slides with a 40 × 20 mm² cover slip and analyzed under an Olympus BX50 polarized light microscope at 1000×. The whole slide was analyzed for each sample in order to detect rare taxa. Selected samples were smeared on a circular glass slide, attached with graphite tape to an aluminum stub, sputter-coated with Cr and analyzed in secondary electron mode under the Zeiss 500 Scanning Electron Microscope (SEM) at the University of Milano-Bicocca.

The presence and relative abundance of diatoms, silicoflagellates and calcareous nannofossils was assessed for each sample and tabulated (Supplement Material, Appendix 2). The total abundance of each group relative to the remaining sediment was estimated using the categories of Koç & Scherer (1996): D = dominant, > 60%; A = abundant, 20–60%; C = common, 5–20%; F = few, 2–5%; R = rare, < 2%; B = barren. Within each group, the relative abundance of each species was estimated per field of view (FOV) or transect on the slide, as: A =abundant; > 10/FOV; C = common; 1–10/FOV; F = few; 1/10 FOVs; R = rare; ≥ 3 /transect; VR = very rare, 1/transect.

Preservation was indicated for diatoms as: G = good, no evident sign of breakage; M = moderate, common fragments; B = bad, rare intact specimens; VB = very bad, no intact diatoms.

Diatom species concepts follow an extended taxonomy (see Supplement Material, Appendix 1). The biostratigraphic ranges of species are after the Barron Diatom Catalogue (table S1 of Lazarus et al. 2014) and the biozonal schemes are from Barron (2015) for the low-latitudes and from Maruyama & Shiono (2003), updated by Scherer et al. (2007) for the North Pacific mid-latitudes. Silicoflagellate species concepts largely follow the taxonomy developed during DSDP-ODP expeditions, as summarized in Perch-Nielsen (1985a) and updated for some more recently-defined species (see Supplement Material, Appendix 1). The zonation of Bukry (1981) updated by Perch-Nielsen (1985a) is used. Calcareous nannofossil species concepts follow the taxonomy and age of Perch-Nielsen (1985b), updated by Young et al. (2023, Nannotax) and their bioevent calibration follows Raffi (2020).

3.3 Tephra

A volcanic ash layer occurs along the P1 section at Cerro Tiza 69 m above the base of the section, hereafter abs (14°40'6.00"S – 75°40'55.00"W). This tephra layer, named CTZ-T324, was sampled avoiding weathered material and contamination by foreign particles, focusing on the base of the layer where biotite phenocrysts are concentrated.

The ash particles were analyzed after smear-slide preparation under a Leica polarized optical microscope. A grain-size analysis was performed through a Malvern Mastersizer 2000E™ Laser Granulometer at

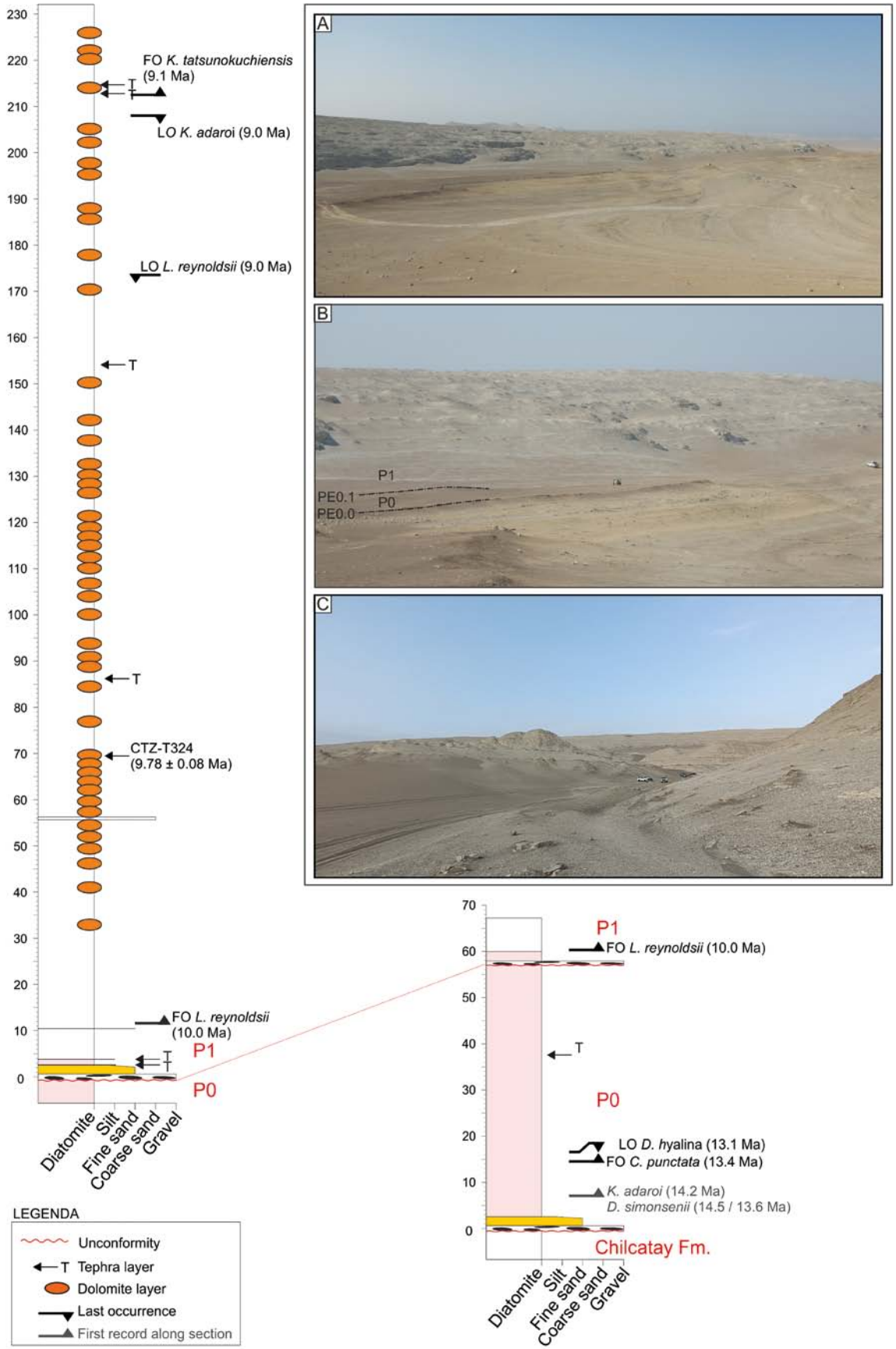
A
B
C
P1
PE0.1
PE0.0
P0
FO K. tatsunokuchiensis (9.1 Ma)
LO K. adaroi (9.0 Ma)
LO L. reynoldsii (9.0 Ma)
T
CTZ-T324 (9.78 ± 0.08 Ma)
FO L. reynoldsii (10.0 Ma)
Diatomite
Silt
Fine sand
Coarse sand
Gravel
LO D. hyalina (13.1 Ma)
FO C. punctata (13.4 Ma)
K. adaroi (14.2 Ma)
D. simonsenii (14.5 / 13.6 Ma)
Chilcatay Fm.
LEGENDA
Unconformity
Tephra layer
Dolomite layer
Last occurrence
First record along section

Fig. 3. Stratigraphic sections of P0 and P1 in the area of Cerro Tiza and location of the identified diatom bioevents and of the dated tephra layer. Panel: field photos **A**) on the southern flank of Cerro Tiza; **B**) detail of A, indicating the base of P0 (PE0.0) and the base of P1 (PE0.1) (car for scale on the right side of the photo); **C**) P1 base (cars for scale on top of PE0.1) and strata on the southeastern flank of Cerro Tiza.

the Università di Milano-Bicocca and calculated with the Grain Size Analysis Program GRADISTAT (Blott & Pye 2001).

The tephra sample was wet-sieved with meshes of 500, 250, 125 and 63 µm. A sub-sample of the 125–250 µm fractions was mounted in araldite resin, polished and prepared for electron probe microanalysis (EPMA) to evaluate its suitability for $^{40}Ar/^{39}Ar$ dating. EPMA on biotite and glass shards was performed with a JEOL 8200 Superprobe™ at the Università di Milano, with 15 kV accelerating voltage and 5 nA beam current. The beam diameter was 3 µm for biotite phenocrysts and 10 µm for glass shards.

Finally, biotite phenocrysts were carefully hand-picked under a stereomicroscope and irradiated in the nuclear reactor at the McMaster University, Canada. Following the procedures described by Bosio et al. (2020a), biotites were analyzed with a step-heating method in a NuInstruments™ Noblesse® multicollector noble gas mass spectrometer at the Università di Milano-Bicocca (Fig. 4).

4 Results

4.1 P0 assemblage at Cerro Tiza

Diatoms analyzed at Cerro Tiza (PNC-13-23, PNC24-D1-D5 and CTi-D15, D100) are common (sometimes few) in most P0 samples from Cerro Tiza (PNC) and display a moderate preservation: only a few intact valves are found within common fragments. No diatoms were found along the P0 sections previously sampled at different locations in the Ica River Valley. The PNC diatom assemblage is dominated by common *Thalassionema* followed by few to common *Denticulopsis*, rare to common *Chaetoceros* spores, rare to few *Crucidenticula*, *Actinoptychus*, *Paralia*, *Grammatophora*, *Thalassiosira*, *Koizumia* (Figs. 5, 6, 7, 10, 11).

Silicoflagellates (Figs. 8, 9) are rare to few (absent in some samples) and dominated by *Distephanopsis crux*. Minor species are mainly represented by cruxoid forms with a square basal ring with bent sides, identified as *Distephanopsis slavnicii*. This is always associated with a dictyochid form, characterized by a similarly-sized square basal ring with bent sides, displaying fibuloid, asperoid or medusoid apical morphology and thus identified as variants of *Dictyocha subarctios*, even though a clear resemblance to *Distephanopsis slavnicii* is evident.

Among the stratigraphic markers:

- *Denticulopsis hyalina* (14.9–13.1 Ma) is present from the base of the section up to 16 m abs (Fig. 3);
- *Denticulopsis simonsenii* (14.5 in the North Pacific/13.6 Ma in the equatorial Pacific – 8.7 Ma) and *D. vulgaris* are absent in the basal layers and appear at about 7 m abs;
- *Crucidenticula nicobarica* (15.1–12.3 Ma) is present, although with a few specimens, throughout the section;
- *Crucidenticula punctata* (13.4–11.4 Ma) is present from 14.5 m abs to the top of the section (Fig. 3);
- *Koizumia adaroi* (14.2–9.0 Ma) is sporadically present throughout the section;
- *Thalassiosira praeyabei* (14.5–13.0 Ma) is sporadically present inthe lower part of the section, *T. yabei* (13.5–8.3 Ma) is sporadically present from mid-section and rare occurrences of *Thalassiosira perispinosa* (FO 14.9 Ma, Barron et al. 2013) are recorded;
- *Coscinodiscus lewisianus* (26.9–12.9 Ma) occurs sporadically throughout the section;
- *Actinocyclus ingens* (18.2–7.8 Ma) occurs sporadically through the section;
- *Lithodesmium californicum* (13.5–6.8 Ma) is sporadically present throughout the section;
- a small *Lithodesmium*, characterized by strongly curved sides and apices, that is similar to *Lithodesmium minusculus* (10.5–4.8 Ma) also occurs and precedes the Late Miocene marker *L. reynoldsii*;
- one specimen of *Actinocyclus ellipticus* (14.0–0 Ma) was recorded at the base of the section, but can be considered as extremely rare;
- *Corbisema triacantha* (LO ~11.2 Ma at the top of the *Corbisema triacantha* zone) is present in a few samples along the section;
- *Cannopilus* sp. and *Stephanocha speculum* var. *hemisphaericum*, typical taxa of the lower *C. tria-*

cantha zone, are present in a few samples along the section.

4.2 P1 assemblage on the western side of the Ica River Valley

Microfossils were analyzed and compared from sections measured at Cerro Tiza (CTZ-278-527; PNC-24-26; PNC24-D6-D10), Cerros Cadenas de los Zanjones (ZANJ-D1-D10 and LA1-15), Cerros la Mama y la Hija (MF-D1-D51) and Ullujaya (UL-D10-D11, D56-D60).

Diatoms are common to abundant (sometimes few) in all samples at Cerro Tiza (CTZ) and display a moderate to good preservation, with common intact valves and common fragments. They range from common to few at Cerros Cadenas de los Zanjones and Cerros la Mama y la Hija, and from barren to common at Ullujaya.

The assemblage is always dominated by *Thalassionema* followed, in order of abundance, by *Denticulopsis*, *Rhizosolenia*, *Chaetoceros* spores, *Delphineis*, *Lithodesmium* and rare *Koizumia*, *Actinocyclus*, *Actinoptychus*, *Nitzschia*, *Paralia*, *Stephanopyxis*, *Thalassiosira*, *Coscinodiscus*, *Azpeitia*, *Diplomenora*, *Rouxia*, *Grammatophora*, *Hemiaulus* (Figs. 5, 6, 7, 10, 11).

Silicoflagellates (Fig. 8, 9) range from rare to few at Cerro Tiza and Cadenas de los Zanjones, but are absent from some samples; they are very rare to absent from Cerros la Mama y la Hija and Ullujaya. The most common species is *Stephanocha speculum*, with common var. *speculum* and var. *pentagona*, with some contribution from var. *bispicata* and var. *hemisphaerica*.

Calcareous nannofossils occur in several intervals throughout the CTZ section, ranging from few to common, but they are absent from the other locations. Their assemblages are dominated by *Reticulofenestra* (*R. pseudoumbilicus*, *R. haqii*, *R. perplexa*, *R. producta*) with rare to few *Coccolithus pelagicus*, *Calcidiscus leptoporus*, *C. tropicus* and *Discoaster variabilis* subsp. *decorus*.

Among the stratigraphic markers:

- *Denticulopsis simonsenii* (14.5/13.6–8.7 Ma), *D. vulgaris* and *D. praekatayamae* (9.6–8.6 Ma) occur throughout the section. *D. vulgaris* and *D. praekatayamae* were tabulated together, due to the difficulty in separating them under the light microscope (see Supplement 1 for discussion); SEM investigation allowed documenting a transitional form between *D. vulgaris* and *D. praekatayamae* in the basal samples of P1;
- *Lithodesmium reynoldsii* (10.0–9.0 Ma) is identified from 15 m abs up to 172 m abs (the top of the measured P1 section is at 232 m abs) (Fig. 3);
- *Koizumia adaroi* (14.2–9.0 Ma) is present from the base up to 119 m abs, although sporadically;
- *Koizumia tatsunokuchiensis* (9.1–2.6 Ma) is sporadically present from 212.5 m abs (Fig. 3);
- *Thalassiosira yabei* (13.5–8.3 Ma) is sporadically present along the section;
- *Nitzschia porteri* (12.2–7.2 Ma) is sporadically present along the section;
- very rare specimens of *Crucidenticula nicobarica* (15.1–12.3 Ma) identified at the base of P1 are interpreted here as reworked;
- *Distephanopsis crux* (LO ~8.0 Ma, top of *D. brevispina* zone) occurs sporadically along the section up to 208 m abs;
- *Dictyocha pulchella* (~19.0 – ~5.5 Ma, *N. ponticula* to lower *D. fibula* zones) is the most significant *Dictyocha* along the whole section but occurs sporadically;
- *Paramesocena apiculata* (~18.0 – ~8.0 Ma, *C. triacantha* and *D. brevispina* zones) is rare but can become common in some samples in the basal layers of P1;
- *Bachmannocena diodon* var. *nodosa* (~11.2 – ~3.0 Ma, *D. brevispina – D. fibula* zones) occurs in a few samples of P1;
- *Reticulofenestra pseudoumbilicus* (17.9–3.7 Ma) occurs along P1, wherever calcareous nannofossils are present;
- *Discoaster variabilis* subsp. *decorus* (13.5–3.7 Ma) is scattered in the basal ~70 m of the section.

4.3 Characterization and age of the tephra layer

The volcanic ash layer CTZ-T324 is comprised of highly vesiculated glass shards, few biotite phenocrysts, and rare amphibole and pyroxene phenocrysts (Fig. 4A). The tephra shows < 10% of non-primary particles. Additionally, biotite phenocrysts are coated by glass, allowing to define it as a product of primary deposition (Fig. 4A). Grain-size analyses show a unimodal distribution, with a high percentage of mud-sized and < 10% of sand-sized particles (Supplement Material, Appendix 3). For this reason, the sample is given the sediment name of coarse silt, belongs to the textural group of mud (Supplement Mate-

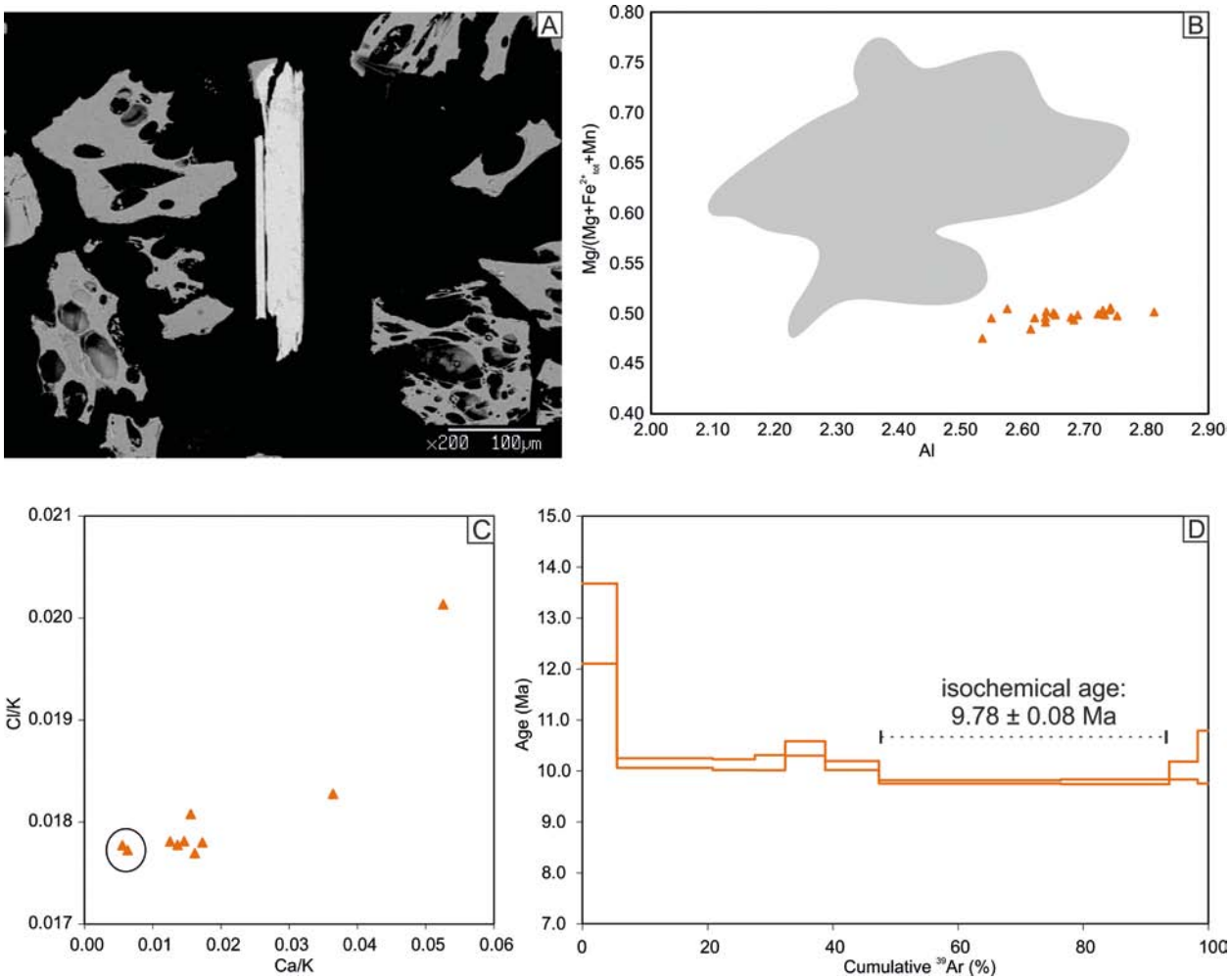

Fig. 4. CTZ-T324 tephra characterization. **A**. BSE image of a well-preserved biotite crystal with glass coating and highly vesiculated glass shards. **B**. Mg/(Mg+Fe^{2+}_{tot}+Mn) vs Al diagram showing biotite composition of the analyzed tephra. The gray field indicates the composition of the volcanic ash layers in the P1 allomember of the Pisco Formation. **C**. Cl/K vs. Ca/K diagram built on irradiation-produced $^{38}Ar/^{39}Ar$ and $^{37}Ar/^{39}Ar$ ratios. The black circle indicates isochemical steps 7 and 8 used for calculating the final age. **D**. Age spectrum of the dated tephra. The dashed line indicates steps 7 and 8, i.e., the steps that better approximates the Ar release from the unaltered biotite.

rial, Appendix 3), and can be classified as extremely fine ash following White & Houghton (2006).

Glass shard analyzed by EPMA indicate a rhyolitic composition and show no evidence of strong alteration; the low totals can be attributed to moderate post-depositional hydration in the marine environment (Bosio et al. 2020a, Villa & Bosio 2023) (Supplement Material, Appendix 3). Biotite shows an Al-rich composition and a slightly low Mg/(Mg + Fe^{2+}_{tot} + Mn) with respect to other P1 tephra (Fig. 4B). Several peraluminous magmas were erupted during the Late Miocene in the Central Andes (Caffe et al. 2012), and some peraluminous tephra reached the East Pisco Basin (Bosio et al. 2020c). Potassium loss is revealed by the alkali site occupancy between 1.72 and 1.88 apfu (atoms per formula unit), lower than the stoichiometric value of 2 apfu (Supplement 3), i.e., it is slightly altered but still suitable for $^{40}Ar/^{39}Ar$ dating. Indeed, the K concentration calculated from the ^{39}Ar release is substoichiometric (Supplement Material, Appendix 3). As discussed in more detail by Villa & Bosio (2023), micas from marine tephra layers in the East Pisco Basin are affected by slight alteration. All the isochrons calculated with different subsets of steps are over dispersed (MSWD>1); an isochemical age is calculated from the weighted average of the two steps

with the lowest Ca/K, steps 7 and 8, since the stoichiometry of biotite does not admit the presence of Ca. This final age is 9.78 ± 0.08 Ma (Fig. 4C, D) (Supplement Material, Appendix 3). The final age estimate is given with a 2σ uncertainty, which takes into account different sources of uncertainty.

5 Discussion

5.1 Age and stratigraphic architecture of the Pisco Formation in the Ica River Valley

In the Ica River Valley, the Pisco Formation crops out as a gently dipping monocline, onlapping on the basement towards the NNE (Di Celma et al. 2022), defining a paleo-basin deepening towards the SSW.

The P0 sequence displays a pronounced wedge-like geometry, showing a maximum thickness of ~40 m at Cerro las Tres Piramides and ~55.5 m at Cerro Tiza, thinning towards Cerro la Bruja where it is not present. While in the Ullujaya area its thickness decreases northeastward likely due to progressive onlap and loss of successively younger beds at the base (Di Celma et al. 2017), in the area of Cerro Tiza erosion at the top can be inferred from satellite images and biostratigraphic data.

Significant lateral facies changes occur within P0, following the south-southwestward paleo-basin deepening: fine- to very coarse-grained, cross-stratified, macrofossil-rich nearshore calcarenites occur in the Cerro Submarino-Ullujaya area (Di Celma et al. 2017), fine-grained siltstones lacking microfossils are present southwestward at Cerros la Mama y la Hija, whereas fine-grained offshore diatomaceous siltstones dominate the southernmost outcrops at Cerro Tiza.

The fossil content reflects such facies changes: the microfossil-barren calcarenites contain mollusks and barnacles, while the diatomaceous siltstones display abundant diatoms and silicoflagellates.

Dating the P0 sequence had thus far been impeded by the coastal nature of the sediments, the absence of microfossils, and the lack of datable ash layers. The age of P0 was thus only constrained by strontium isotope stratigraphy on barnacle and oyster shells and shark teeth to 14.7–12.6 Ma at Cerro Submarino (Bosio et al. 2020b, 2022). The identification of a diatomaceous succession at Cerro Tiza has enabled the use of biostratigraphic markers.

Based on the presence of *Denticulopsis hyalina* (0–16 m abs) and the occurrence of *Denticulopsis simonsenii* (7–41 m abs) and *Koizumia adaroi* (7–39 m abs), the lower 16 m are constrained between 14.2 and 13.1 Ma; this age is supported by the occurrence of *Crucidenticula punctata* (14.5–55 m abs), *Crucidenticula nicobarica*, rarer *Thalassiosira perispinosa* and *Th. praeyabei* and other species that have a longer range.

Among silicoflagellates, the presence of *Cannopilus* associated with multi-windowed *Stephanocha speculum* is suggestive of the *Cannopilus schulzii* subzone (~18 – ~13.5 Ma), even if their range can be also younger. Notably, 4-sided silicoflagellates with strongly bent sides and displaying both cruxoid (e.g., *Distephanopsis slavnicii*) and dictyochid (e.g., *Dictyocha subarctios*) features are reported from a distinct interval within the diatomaceous P0 and are not documented elsewhere in the Pisco Formation.

The upper part of the P0 section (16–55.5 m abs) is constrained to be older than 12.9 Ma by the presence of *Coscinodiscus lewisianus*, a few specimens of which occur up to the top of the section, even if the presence of *Crucidenticula nicobarica* (LO 12.3 Ma) and *C. punctata* (LO 11.4 Ma) could support potentially younger ages at the top. Among silicoflagellates, the occurrence of *Corbisema triacantha* is noteworthy: the few recorded individuals represent the final occurrences of this long-ranging species, widely present in the older strata of the Pisco Basin, before its global extinction at ~11.2 Ma.

Overall, the P0 sequence is almost completely contained in the *Coscinodiscus lewisianus* low-latitude diatom zone, or in the upper part of *Denticulopsis hyalina* and in the *Crucidenticula nicobarica* North-Pacific mid-latitude zones. It belongs to the *Corbisema triacantha* silicoflagellate tropical-subtropical zone

Fig. 5. Diatoms: **1–4**) *Denticulopsis hyalina*: 1, common form; 2, elongated form; 3, slightly tilted; 4, girdle view of 2 complete individuals; **5**) *D. simonsenii*; **6–10**) *D. vulgaris*, 7, normal form; 8, with slightly curved sides; 9, short form; 10, girdle view; 10, slightly tilted; **11**) *D. vulgaris–D. praekatayamae* transitional form, with curved sides; **12, 13**) *Lithodesmium californicum*; **14, 15**) *L. reynoldsii*, **16–18**) *Lithodesmium* cf. *minusculum*, with strongly curved sides; 19) *Lithodesmium* cf. *californicum*.

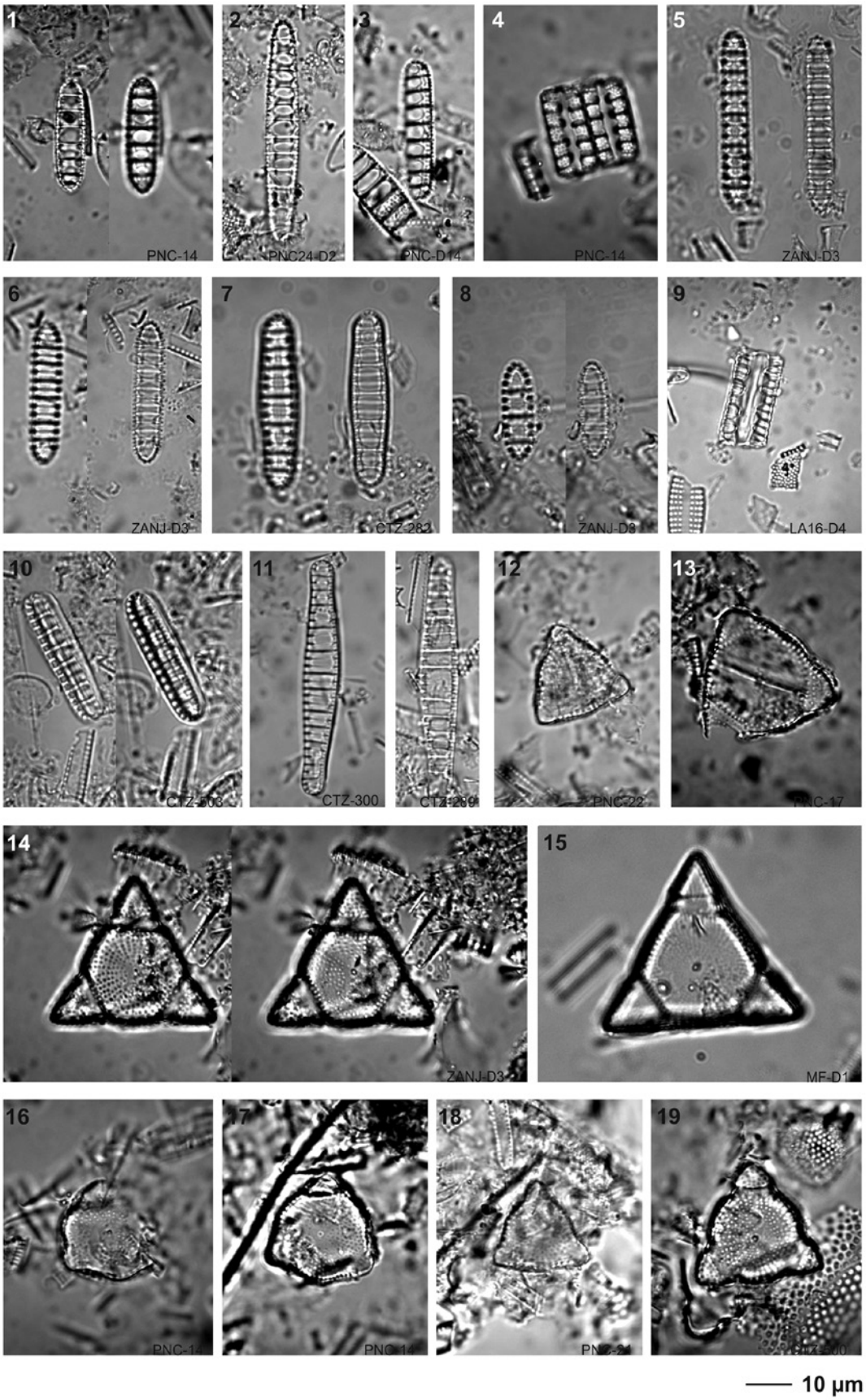
1
PNC-14
2
PNC24-D2
3
PNC-D14
4
PNC-14
5
ZANJ-D3
6
ZANJ-D3
7
CTZ-282
8
ZANJ-D3
9
LA16-D4
10
CTZ-508
11
CTZ-300
CTZ-300
12
PNC-22
13
PNC-17
14
ZANJ-D3
15
MF-D1
16
PNC-14
17
PNC-14
18
19
10 µm

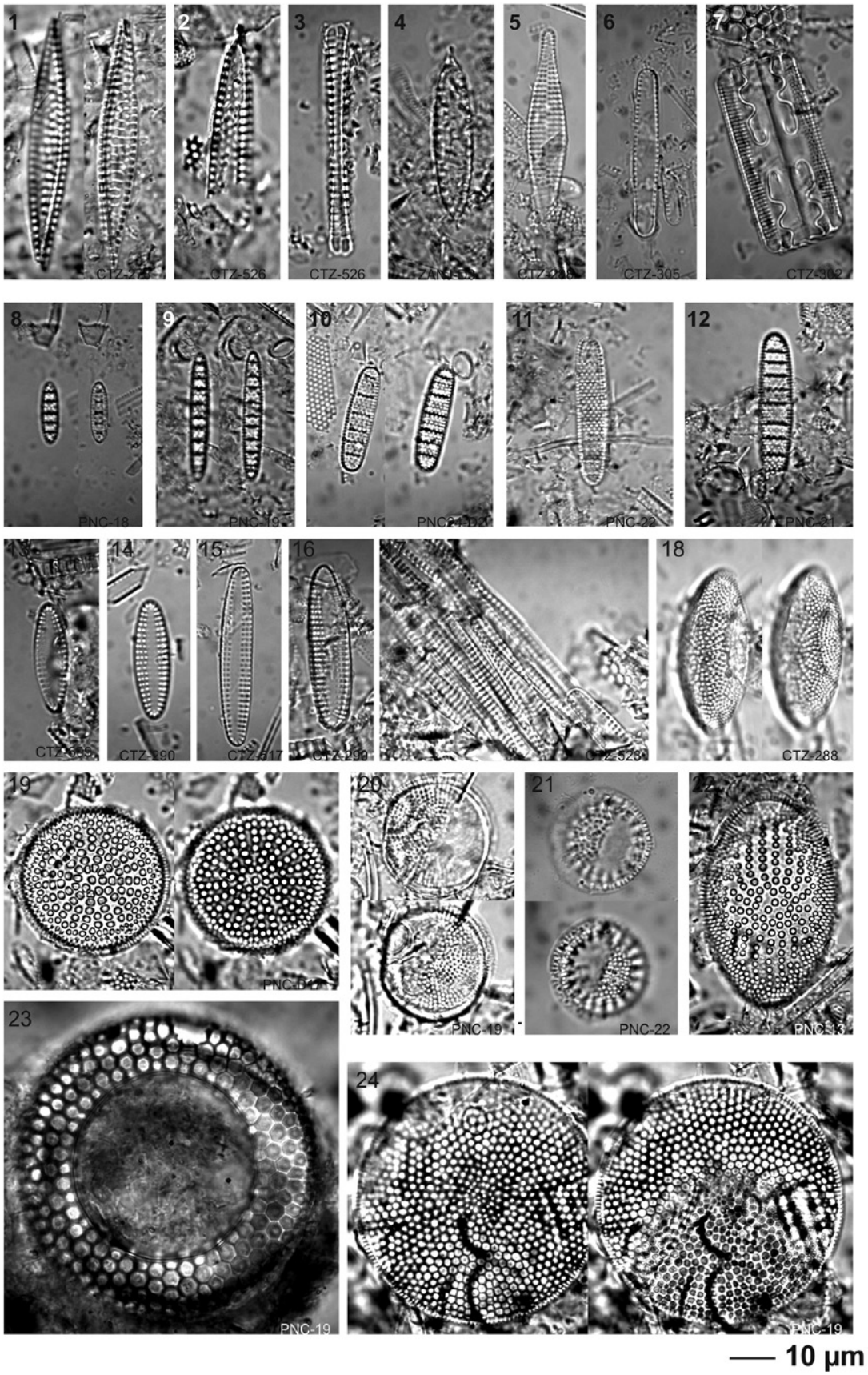
1
CTZ-2
2
CTZ-526
3
CTZ-526
4
5
6
CTZ-305
7
CTZ-302
8
PNC-18
9
PNC-19
10
PNC-21
11
PNC-22
12
PNC-21
13
14
CTZ-290
15
16
CTZ-290
17
18
CTZ-288
19
20
PNC-19
21
PNC-22
22
23
PNC-19
24
PNC-19
10 µm

Fig. 6. Diatoms: **1**) *Koizumia adaroi*; **2–4**) *K. tatsunokuchiensis*, 2, elongated form (broken); 3, girdle view; 4, short form; **5**) *Rhaphoneis* sp., **6**) *Thalassionema* sp.; **7**) *Grammatophora* sp.; **8, 9**) *Crucidenticula nicobarica*, **10–12**) *Crucidenticula punctata*; **13, 14**) *Delphineis simbirskiana*; **15–17**) *Delphineis sachalinensis*; **18**) *Actinocyclus ellipticus*; **19**) *Actinocyclus ingens*; **20**) *Thalassiosira perispinosa*; **21**) *Thalassiosira cf. T. urahoroensis*; **22**) *Coscinodiscus lewisianus*; **23**) *Craspedodiscus coscinodiscus*; **24, 25**) *Azpeitia salisburyana*

and in particular it likely falls within the *Cannopilus schulzii* sub-zone, due to the common abundance of *Cannopilus* spp.and *Stephanocha speculum* var. *hemisphaerica* and the absence of *Dictyocha stauracantha* whose first occurrence marks the base of the nominal sub-zone.

Recent work by DeVries et al. (2021) described P0-correlative members of the Pisco Formation in the Laberinto area. Their diatom assemblages have several species in common with our PNC section (*D. hyalina*, *D. simonsenii*, *C. nicobarica*, *C. punctata*, *C. lewisianus*, *A. ingens*, *Th. praeyabei*, *Th. perispinosa*, *A. octonarius*, *C. triacantha*). They also found coastal age-diagnostic species of *Delphineis* (*D. angustata*, *D. biseriata*, *D. penelliptica*) that agree with a nearshore setting for their fine-to coarse-grained sandstones. The lack of *Delphineis* in our samples and the scarce presence of other coastal taxa (*Actinoptychus*, *Grammatophora*, *Paralia*, *Rhaphoneis* and *Stephanopyxis*) likely indicate a slightly deeper setting for the Cerro Tiza P0 sediment succession. The other species mentioned by DeVries et al. (2021) (*Actinoptychus minutus*, *A. vulgaris*, *Azpeitia nodulifera*, *A. vetustissima*, *Cavitatus jouseana*, *Cestodiscus kugleri*, *C. pulchellus*, *Coscinodiscus gigas*, *Denticulopsis lauta*, *Hemiaulus polymorphus*, *Nitzschia* aff. *N. denticuloides*, *Rhizosolenia miocenica*, *Stephanopyxis schenckii*, *Thalassiosira flexosa*, *Th. leptopus*, *Th. mioplicata*, *Th. tappanae*) were not recorded along our section at Cerro Tiza.

Additionally, our P0 samples display frequent occurrences of *Denticulopsis vulgaris*, which has not been mentioned from the Laberinto area (but see Supplement Material, Appendix 1). It is worth noting that the first occurrence of *D. vulgaris* is time-transgressive (13.5 Ma in the North Pacific to ~10.0 Ma in the equatorial Pacific, Yanagisawa & Akiba 1990) and the species first appears in our section along with *Denticulopsis simonsenii* (FO 14.5 in the North Pacific, but 13.6 in the equatorial Pacific), as confirmed by SEM analyses, therefore possibly pre-dating its own North Pacific occurrence.

Overall, our estimate for the age of the P0 sequence at Cerro Tiza (from 14.2 to 12.9 Ma) is closely similar to that obtained by means of SIS (Bosio et al. 2020b, 2022) and for the P0 correlative strata at Laberinto (14.4–12.8 Ma, DeVries et al. 2021). Uncertainty remains on the first occurrence of *D. simonsenii*,which is time-transgressive at different latitudes (14.5 Ma in the North Pacific, 13.6 Ma in the equatorial Pacific) and of *D. vulgaris* which is still loosely constrained. A slightly different age of P0 in the two localities is in any case to be expected, given the time-transgressive nature of the basal layers of the stratigraphic sequences.

The geometry of the P1 sequence is similar to that of P0: it becomes progressively thicker towards the southwest, ranging from 42 m at Cerro la Bruja (Bosio et al. 2019, Di Celma et al. 2022) to 66 m at Cerros la Mama y la Hija (Bosio et al. 2020a), 95 m at Cerros Cadenas de los Zanjones and > 230 m at Cerro Tiza, the latter lacking its upper portion due to late erosion after the final uplift.

The P1 stratal unit also displays significant facies changes, ranging from nearshore bioclastic-rich microfossil-poor calcarenites at Cerro la Bruja to diatomaceous siltstones at Cerros la Mama y la Hija to diatomites at Cerros Cadenas de los Zanjones and Cerro Tiza (Fig. 3). The microfossil content reflects such lateral facies changes: diatoms are rare at Cerro la Bruja, few to common at Cerros la Mama y la Hija and common to abundant at Cerros Cadenas de los Zanjones and Cerro Tiza. The latter section also contains few to common calcareous nannofossils, that represent their only record in P1 sediments. Calcareous nannofossils were in fact absent elsewhere due to missing deposition in nearshore areas or to lack of preservation.

The base of the P1 sequence has been previously defined at northern localities of the Ica River Valley through combined diatom biostratigraphy and absolute tephra dating at Cerro Colorado, Cerro los Quesos (Garibodi et al. 2017), Cerros la Mama y la Hija and Cerros Cadenas de los Zanjones (Bosio et al. 2020a).

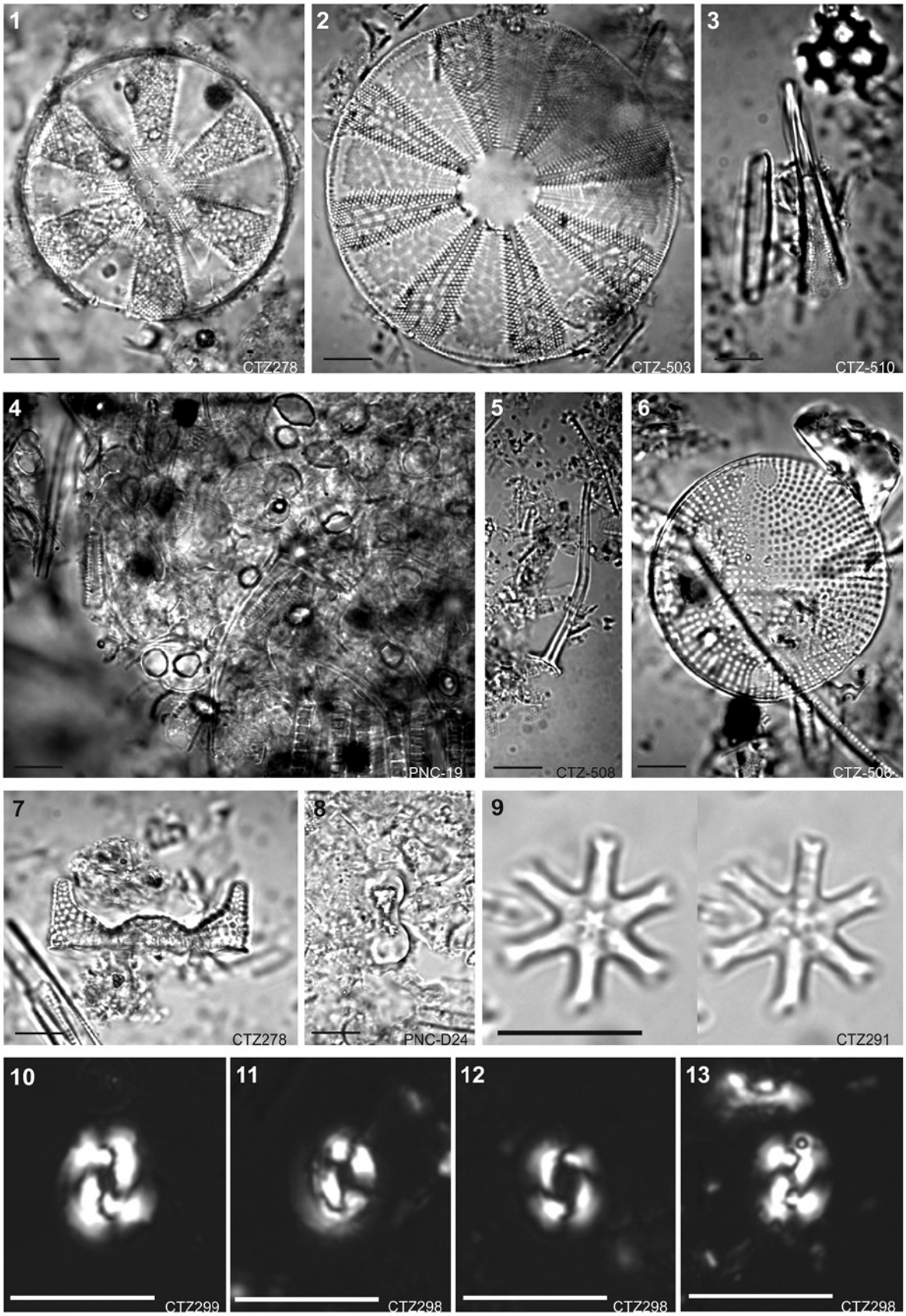
1
CTZ278
2
CTZ-503
3
CTZ-510
4
PNC-19
5
CTZ-508
6
CTZ-508
7
CTZ278
8
PNC-D24
9
CTZ291
10
CTZ299
11
CTZ298
12
CTZ298
13
CTZ298

Fig. 7. Diatoms, phytolith and calcareous nannofossils: **1, 2**) *Actinoptychus* sp.; **3**) *Rhizosolenia* sp.; **4**) diatom mate, with abundant *Chaetoceros* resting spores and setae; **5**) *Chaetoceros* seta; **6**) *Diplomenora* sp.; **7**) *Eucampia* sp.; **8**) bilobate phytolith (cf. Piperno et al. 2006); **9**) *Discoaster variabilis* var. *decorus*; **10**) *Reticulofenestra pseudoumbilicus*; **11**) *Coccolithus pelagicus*; **12**) *R. haqii*; **13**) *R. perplexa.* Scale bar = 10 µm.

All data converge to indicate a basal age of P1 at ~9.5 Ma. Although DeVries & Frassinetti (2003) and DeVries & Jud (2018) assumed as plausible an age of 12.5–12 Ma for the basal P1 layers at Cerros la Mama y la Hija and the nearby Cerro Yesera de Amara, based on the absence of younger species along with the presence of species whose range is compatible with such an old age, they do not record any species that allows for an unequivocal constrain. On the contrary, we find *Lithodesmium reynoldsii* at the base of P1 in our section at Cerros la Mama y la Hija (MF-D1, 14°36' 41.3"S; 75°40'21.4"W), indicating that the base of P1 there is younger than 10 Ma.

Recent work by DeVries et al. (2021) in the Laberinto area has described a P1-correlative sequence, which they locally referred to as "Mature Formation", that has a diatom assemblage corresponding to the diatom assemblage of P1, with important markers being represented by *Lithodesmium reynoldsii* and *Denticulopsis praekatayamae* (indicated as *D. katayamae*, but their species concept includes also *D. praekatayamae* as used by Gariboldi et al. 2017).

At Cerro Tiza, we document the first occurrence of *L. reynoldsii* (FO at 10.0 Ma) at 12 m abs, thus implying that the base of P1 is indeed (slightly) older than 10 Ma. Also, the most abundant form of *Denticulopsis* in our lowermost samples (but also at the base of Cerros la Mama y la Hija) is represented by *D. vulgaris* and by a transitional *D. vulgaris*/*D. praekatayamae* form (Figs 5, 10, 11) that probably precedes the first occurrence of typical *D. praekatayamae* at 9.6 Ma.

We did not find *Denticulopsis dimorpha* which in turn has been reported by DeVries et al. (2021) from the Mature Formation.

Delphineis sachalinensis, indicated as a significant component of the Mature Formation, is present with variable abundance along our sections of P1. We separated the more elongated *D. sachalinensis* from the more oval-shaped *Delphineis simbirskiana* that co-occurs in most P1 samples (see Supplement Material, Appendix 1 and Fig. 6). Both forms were reported by Mertz (1966) from the Pisco Basin (although with different names, see Supplement Material, Appendix 1). Among the silicoflagellates, the occurrence of long-ranging *Paramesocena apiculata* is noteworthy, as it occurs in significant abundances in some samples; *D. crux* is an important marker (LO ~8.0 Ma) that is present throughout the succession.

Among the calcareous nannofossils, *Reticulofenestra pseudoumbilicus* (17.95–3.7 Ma) occurs throughout the Cerro Tiza succession, wherever calcareous nannofossils are present. Its occurrence is likely constrained below the base of its global interval of absence (paracme zone or interval of absence from 8.8 to 7.1 Ma, Backman et al. 2012).

Finally, CTZ-T324 (9.78 ± 0.08 Ma), collected at 69 m abs at Cerro Tiza, represents the oldest tephra dated so far in the Pisco Formation, as compared to the P1 tephra layers dated at Cerro Colorado (CC-T1b: 9.10 ± 0.04 Ma), at the base of Cerros Cadenas de los Zanjones (ZAN-T6: 9.46 ± 0.05 Ma and LA(16): 9.00 ± 0.02 Ma) and at the Anfiteatro locality (ANF-T1a: 9.31 ± 0.01 Ma) (Bosio et al. 2020a). Overall, diatom biostratigraphy and the dated tephra layer concur in defining the base of P1 at Cerro Tiza to be around 10.0 Ma: such an old age defines a progressive landward decrease in age of the basal strata of the P1 sequence, due to the northeastwards pattern of coastal onlap.

The age of the top of P1 has been constrained at Cerro los Quesos, Cerros Cadenas de los Zanjones and Cerros la Mama y la Hija by the last occurrence of *D. praekatayamae* a few meters below the top and by absolute dating of one tephra layer at 8.60 ± 0.11 Ma (ZANJ-T3) (Gariboldi et al. 2017, Bosio et al. 2020a, Di Celma et al. 2022), with the last occurrence of

Fig. 8. Silicoflagellates: **1–4**) *Dictyocha pulchella*; **5**) *Dictyocha aspera* subsp. *clinata*; **6–9**) *Stephanocha speculum*: 6, var. *speculum*, 7, var. *pentagona*; 8, var. *bispicata*, 9, var. *hemisphaerica*; **10–12**) *Cannopilus* sp.

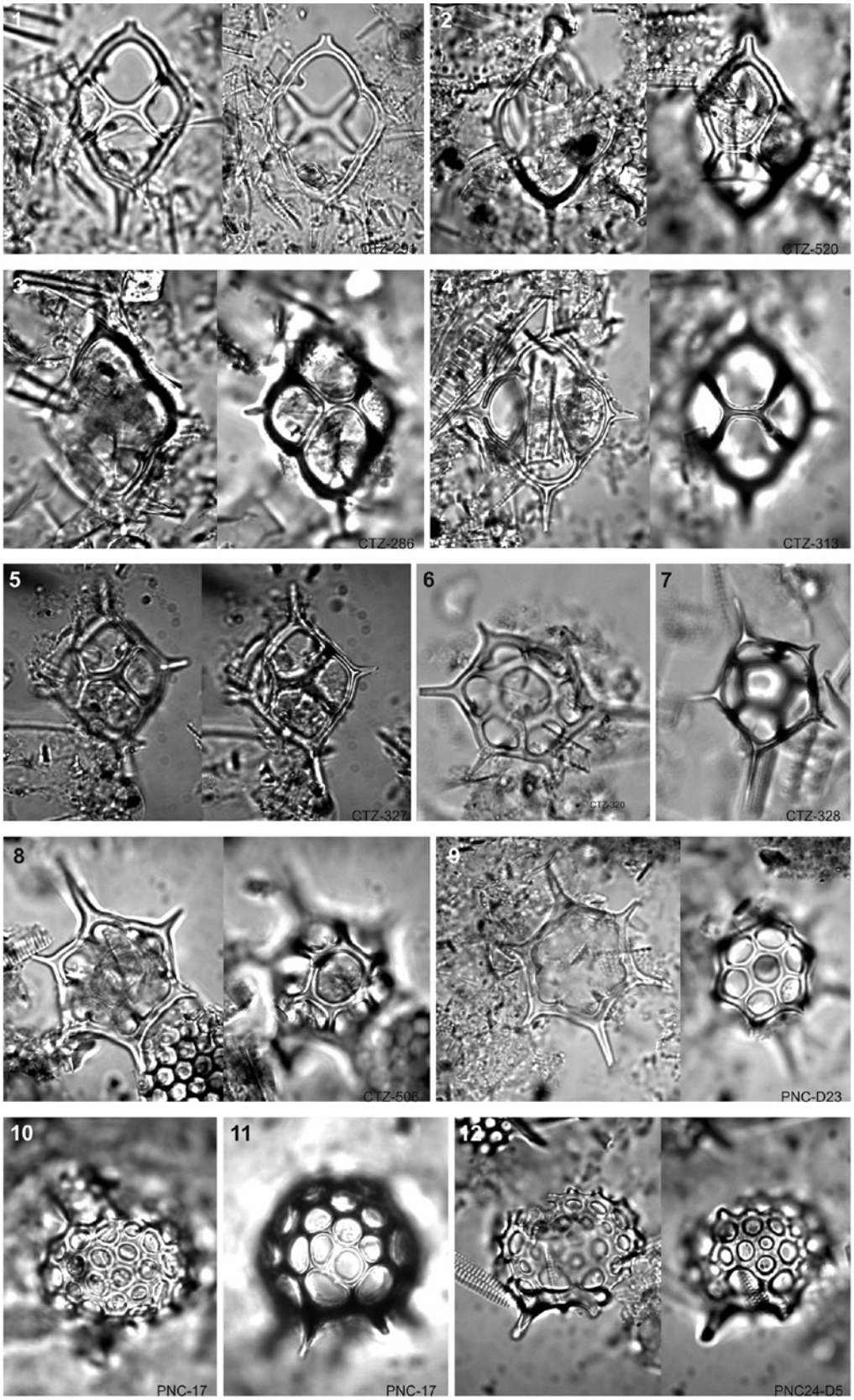
1
CTZ-291
2
CTZ-520
3
CTZ-286
4
CTZ-313
5
CTZ-321
6
CTZ-320
7
CTZ-328
8
CTZ-506
9
PNC-D23
10
PNC-17
11
PNC-17
12
PNC24-D5
10 µm

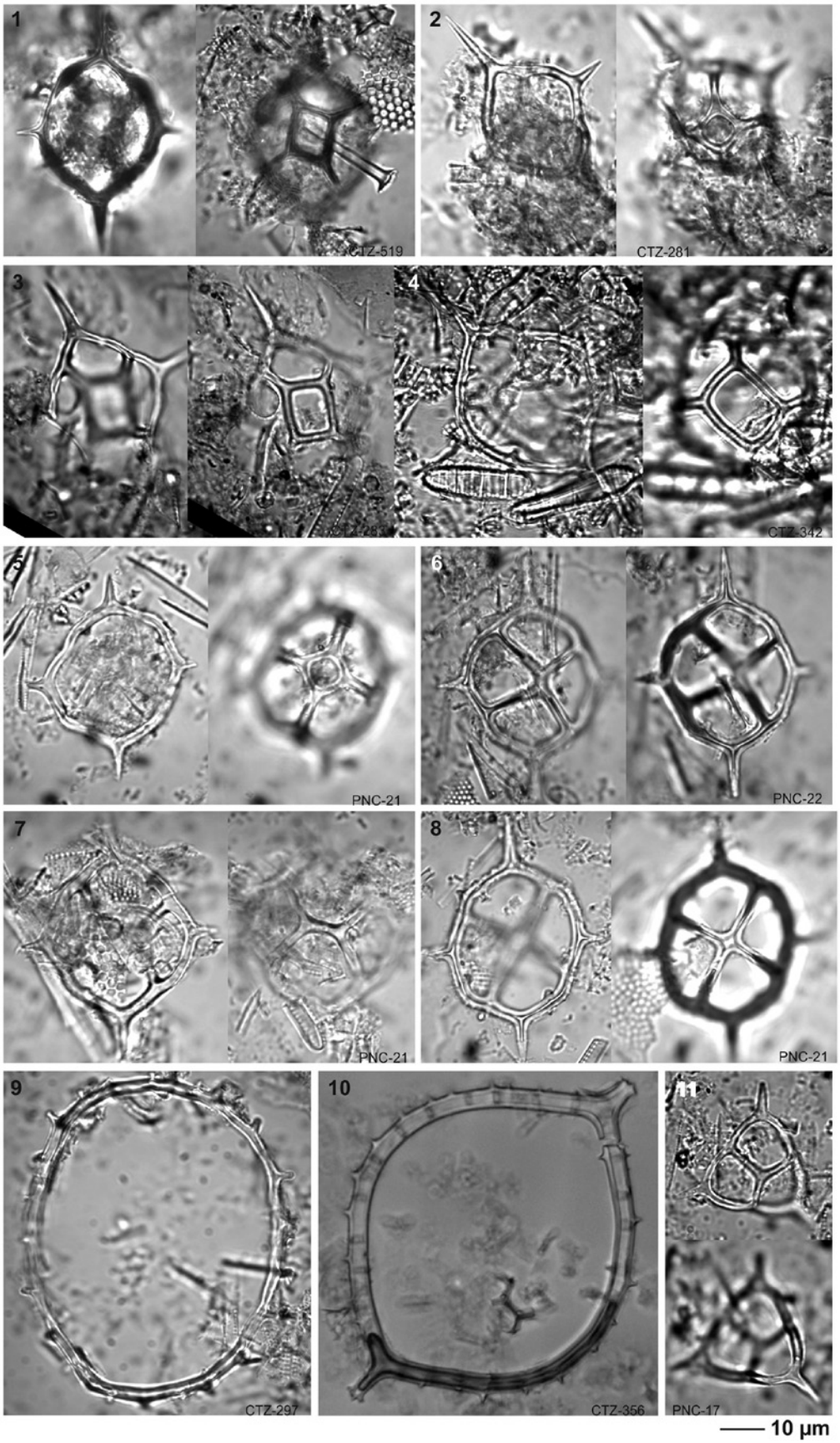
1
CTZ-519
2
CTZ-281
3
4
CTZ-342
5
PNC-21
6
PNC-22
7
PNC-21
8
PNC-21
9
CTZ-297
10
CTZ-356
11
PNC-17
10 µm

Fig. 9. Silicoflagellates: **1–4**) *Distephanopsis crux*, 1–2, normal forms; 3, with slightly elongated and rotated apical ring, 4, with strongly elongated apical ring; **5**) *Distephanopsis slavnicii*; **6–8**) *Dictyocha subarctios*, 6, normal form, 7, asperoid form, 8, medusoid form; **9**) *Paramesocena apiculata*; **10**) *Bachmannocena diodon* var. *nodosa*; **11, 12**) *Corbisema triacantha*.

L. reynoldsii (9.0 Ma) being identified a few meters below. At Cerro Tiza, *L. reynoldsii* occurs, although scattered, up to 173.5 m abs, thus constraining the main part of the section to be between 10.0 Ma and 9.0 Ma old, as confirmed by the scattered presence of *Koizumia adaroi* (LO 9.0 Ma) up to 208 m abs and by the occurrence of *K. tatsunokuchiensis* (FO 9.1 Ma) a few meters above. Rare *Denticulopsis simonsenii* and *D. praekatayamae* are still present at the top, suggesting that the upper layers of the P1 sequence are locally older than 8.6 Ma. Also, the presence of *Reticulofenestra pseudoumbilicus* in the upper layers would further constrain the age of the top to prior its interval of temporary absence starting at 8.8 Ma. Indeed, the upper layers of P1 and the P2 sequence above are lacking at Cerro Tiza: they were probably eroded subaerially after the final uplift of the basin.

Overall, the P1 sequence is constrained to the upper part of the *Actinocyclus moronensis* and to the *Thalassiosira yabei* low-latitude diatom zones, or in the *Denticulopsis dimorpha* and *D. katayamae* North-Pacific mid-latitude zones and belongs to the *Dictyocha brevispina* silicoflagellate tropical-subtropical zone.

The age of the P0-P1 unconformity (12.9 Ma to nearly 10 Ma) as recorded at Cerro Tiza (this work) and in the Laberinto area (DeVries et al. 2021) corresponds to the major drop in sea-level centered at 11.7 Ma (Mi-5 of Miller et al. 1991, 1998, as calibrated by Boulila et al. 2011) but might also include the minor positive oxygen isotope shifts at 12.9 Ma (Mi-4) and 10.3 Ma (Mi-6). Extended periods of low sea-level would imply a prolonged interval of non-deposition, as suggested in Di Celma et al. (2018a). However, evidence of an ash bed dated through U/Pb on zircons at 11.98 Ma at Ladera de Lisson (DeVries et al. 2021), approximately 31 km to the south-east of our study area and a few km east of the Laberinto area, implies a shorter hiatus, and could indicate more extended deposition cut by major erosional events, as discussed by DeVries et al. (2021). Indeed, due to the time-transgressive nature of the coastal onlap at the base as well as the local extent of erosion at the overlying unconformity, the oldest and youngest sediments of a depositional sequence may show age variations throughout the basin.

5.2 Paleoclimatic and Paleoceanographic constraints

During the second half of the Miocene (Fig. 3), the Earth's climate saw a remarkably warm interval (the Miocene Climatic Optimum, ca. 17–14 Ma) followed by an abrupt cooling (the Middle Miocene Climate Transition, ca. 14 Ma) after which the global temperatures remained distinctly colder than they were before (Westerhold et al. 2020). These keystone episodes of the Earth's past climate are recorded in the studied succession, though in a way that is intimately connected to the geodynamic and oceanographic evolution of the southeastern Pacific margin.

Crucially, the latter is now home to the northward-flowing Humboldt Current, which includes surface and subsurface currents that bring deep, cold, nutrient-rich waters from Antarctica to Peru, thus sustaining high levels of productivity along the western coast of South America (Penven et al. 2009, Chavez & Messié 2009, Karstensen & Ulloa 2009). Also known as the Peru-Chile Current, the Humboldt Current is thought to have begun during the Eocene or Oligocene, following major regional events such as the rise of the Andes and the opening of the Drake Passage (Marty et al. 1988), but its age and origin still remain poorly constrained.

The diatom assemblages of the Middle Miocene P0 include diatom species that are regarded as typical of either the Pacific low latitudes (e.g., *Crucidenticula* spp. and *Thalassiosira yabei*) or the North Pacific mid

Fig. 10. SEM images of diatoms: **1, 2**) *Denticulopsis hyalina*; **3, 4**) *D. simonsenii*; **5, 6**) *D. vulgaris*; **7, 8**) *D. vulgaris/D. praekatayamae* transitional form.

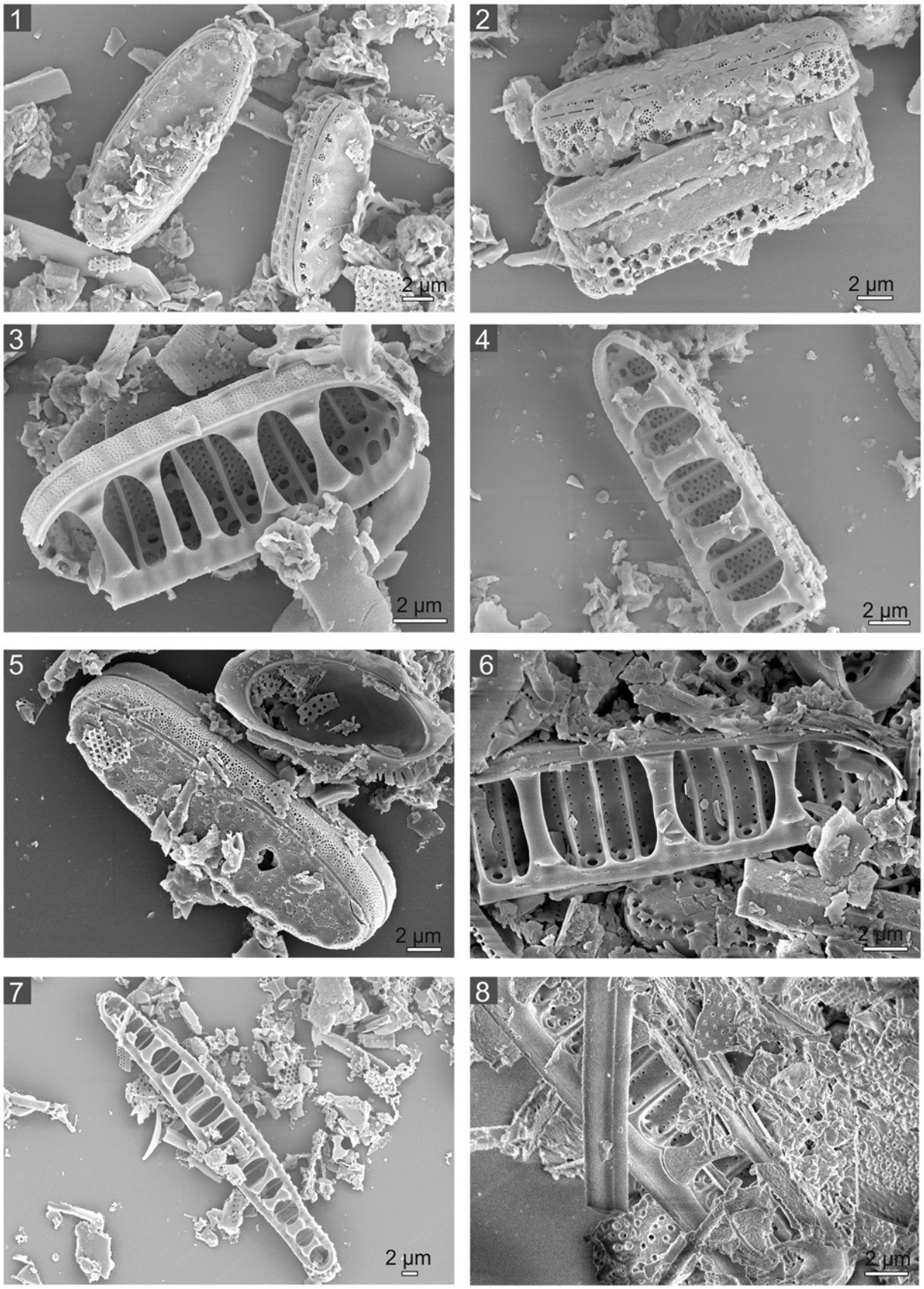
1
2 µm
2
2 µm
3
2 µm
4
2 µm
5
2 µm
6
2 µm
7
2 µm
8
2 µm

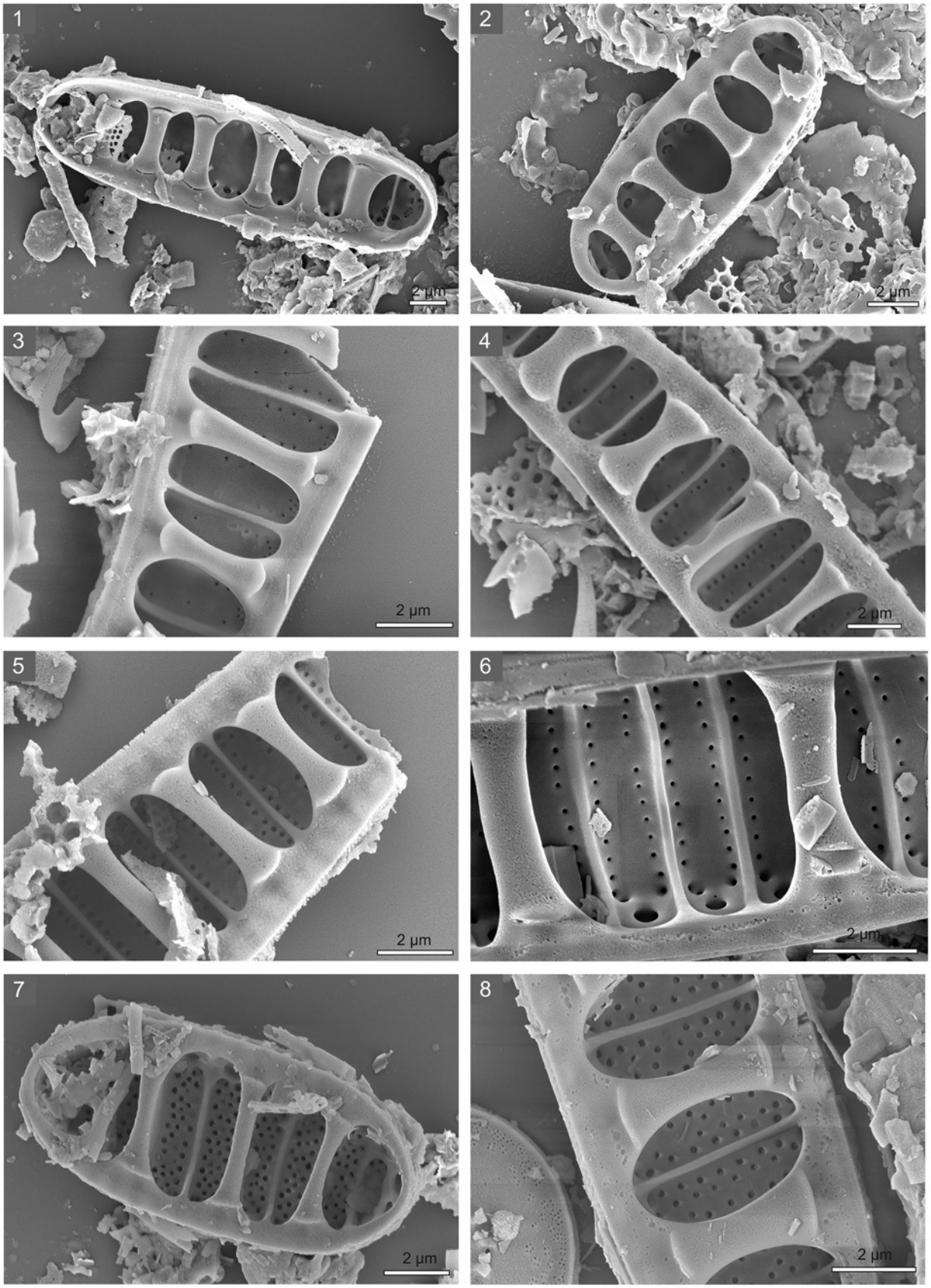
1
2 µm
2
2 µm
3
2 µm
4
2 µm
5
2 µm
6
2 µm
7
2 µm
8
2 µm

Fig. 11. SEM images of diatoms: **1, 2**) *Denticulopsis hyalina*; **3**) *D. praekatayamae*; **4**) *D. vulgaris*/*D. praekatayamae* transitional form; **5, 6**) *D. vulgaris*; **7, 8**) *Denticulopsis simonsenii.*

latitudes (e.g., *Th. praeyabei* and *Denticulopsis* spp.), thus suggesting an influence of cool waters related to upwelling, as proposed by DeVries et al. (2021) for the P0-correlative strata in the Laberinto area. Indeed, upwelling is supported by the common presence of *Thalassionema* (mostly *T. nitzschioides*) and *Chaetoceros* resting spores throughout the succession, these genera being indicative of high nutrient availability.

The P0 depositional setting was relatively shallow at Cerro Tiza, as indicated by the presence of coastal diatom genera (*Actinoptychus*, *Grammatophora*, *Paralia*, *Rhaphoneis* and *Stephanopyxis*) and phytoliths, even though the absence of coastal *Delphineis* is probably indicative of slightly deeper conditions compared to those recorded in the Laberinto area.

The invertebrate assemblages that occur in the very shallow-water P0 strata exposed at Cerro Submarino (Bosio et al. 2020b) include architectonicid, conid and cypraeid gastropods, the ficid species *Ficus distans*, and the only coral colony to have ever been found in the East Pisco Basin, all of which indicate warm-water conditions. The fossil vertebrates from the base of the same deposits (Collareta et al. 2021a) also suggest a (sub)tropical, marginal-marine setting connected with the open ocean.

The diatom markers that are found in P1 are mostly mid-latitude North Pacific species, thus suggesting distinctly cooler climate conditions for this Tortonian unit. Intense upwelling is supported by the presence of *Thalassionema* and of *Chaetoceros* spores that are common to abundant throughout the section. Rare to few coastal genera, among which is *Delphineis* (including *D. sachalinensis* and *D. simbirskiana*), do also occur. The vertebrate fossil record of the P1 sequence is also consistent with high productivity in the way it features the coexistence of two apex predators (*Carcharocles megalodon* and *Livyatan melvillei*) as well as a rich and diverse assemblage of piscivores (among which are many taxa of cetaceans, seabirds and sharks) (Collareta et al. 2021a).

Moreover, just like the modern Humboldt Current System, the P1 vertebrate food web was based on sardines (*Sardinops*), which nowadays thrive in the eastern boundary upwelling systems (Collareta et al. 2015, 2017, Lambert et al. 2015). The local disappearance of the snaggletooth shark genus *Hemipristis* at the P0-P1 passage (Bosio et al. 2020b) also suggests that the Pisco waters were cooler during the Tortonian than in Middle Miocene times.

All this paleoecological information and the sedimentological, paleontological and geochemical records of the underlying rocks (e.g., Dunbar et al. 1990, DeVries et al. 2017, Malinverno et al. 2021, Kiel et al. 2023) converge in indicating an overall cooling trend as well as a strengthening of the (proto-)Humboldt Current and related coastal upwelling in the (early) Late Miocene.

6 Conclusions

We documented the earliest phases of deposition of the Pisco Formation from the diatomaceous layers of the P0 sequence at Cerro Tiza and we constrained the age of this stratal package between 14.2 and 12.9 Ma through the presence of the diatom species *Denticulopsis hyalina*, *D. simonsenii* and *Koizumia adaroi* in the lower layers and *Coscinodiscus lewisianus* at the top. Notably, this age assignment is in good agreement with previous age estimates obtained via strontium isotope stratigraphy of P0 at 14.7–12.6 Ma in the central Ica River Valley and coincides with the age inferred for P0-correlative members of the Pisco Formation in the southern portion of the Laberinto area.

We confirm that the base of the P1 sequence is as old as 10 Ma in the deeper paleo-setting of Cerro Tiza. We also document the occurrence of a transitional *Denticulopsis vulgaris*/*D. praekatayamae* form, which probably precedes both the first occurrence of the typical *D. praekatayamae* (FO at 9.6 Ma) and the first occurrence of *Lithodesmium reynoldsii* (FO 10.0 Ma) along the section.

These findings provide better chronological constraints to the depositional sequences of the Pisco Formation and a better understanding of the basin geometry during the late Early and Middle Miocene. This knowledge is crucial for understanding the evolution of the rich marine vertebrate fauna of the Pisco Formation and for unraveling its paleoceanographic context.

Acknowledgements. Special thanks to A. Gioncada, G. Carnevale, P.P. Pierantoni, T.J. DeVries and J. Barron for the stimulating discussions on the Pisco Formation. Thanks to R. Varas-Malca and W. Aguirre for their support in the field. The authors wish to thank V. Barberini, N. Fusi and A. Risplendente for the help with $^{40}Ar/^{39}Ar$ dating, grainsize and microprobe analyses, respectively.
The authors wish to thank the two anonymous reviewers and the Editor, that significantly improved the quality of this manuscript with their comments and suggestions.

Funding

This work was funded by the European Union – NextGenerationEU, Mission 4, Component 2 CUP I53D23002070 006. Financial support was also provided by a grant from the Università di Milano-Bicocca (2022-ATEQC-0018).

References

Backman, J., Raffi, I., Rio, D., Fornaciari, E., & Pälike, H. (2012). Biozonation and biochronology of Miocene through Pleistocene calcareous nannofossils from low and middle latitudes. *Newsletters on Stratigraphy, 45*(3), 221–244. https://doi.org/10.1127/0078-0421/2012/0022

Barron, J. A. (1985). Miocene to Holocene Planktic diatoms. In H. M. Bolli, J. B. Saunders, & K. Perch-Nielsen (Eds.), *Plankton Stratigraphy* (pp. 763–810). Cambridge: Cambridge University Press.

Barron, J. A., Browning, J., Sugarman, P., & Miller, K. G. (2013). Refinement of late-Early and Middle Miocene diatom biostratigraphy for the East Coast of the United States. *Geosphere, 9*(5), 1286–1302. https://doi.org/10.1130/GES00864.1

Belia, E. R., Nick, K. E., Bedoya Agudelo, E. L., & Watkins, D. K. (2019). Earliest Miocene calcareous nannofossil biostratigraphy from the low-latitude Pisco Basin (Peru). *Stratigraphy, 16*(2), 87–105. https://doi.org/10.29041/strat.16.2.87-105

Bianucci, G., & Collareta, A. (2022). An overview of the fossil record of cetaceans from the East Pisco Basin (Peru). *Bollettino della Società Paleontologica Italiana, 61*(1), 19–60.

Bianucci, G., Di Celma, C., Landini, W., Post, K., Tinelli, C., de Muizon, C., . . . Lambert, O. (2016). Distribution of fossil marine vertebrates in Cerro Colorado, the type locality of the giant raptorial sperm whale *Livyatan melvillei* (Miocene, Pisco Formation, Peru). *Journal of Maps, 12*(3), 543–557. https://doi.org/10.1080/17445647.2015.1048315

Bianucci, G., Collareta, A., Bosio, G., Landini, W., Gariboldi, K., Gioncada, A., . . . Di Celma, C. (2018). Taphonomy and palaeoecology of the lower Miocene marine vertebrate assemblage of Ullujaya (Chilcatay Formation, East Pisco Basin, southern Peru). *Palaeogeography, Palaeoclimatology, Palaeoecology, 511*, 256–279. https://doi.org/10.1016/j.palaeo.2018.08.013

Bianucci, G., Benites-Palomino, A. M., Collareta, A., Bosio, G., de Muizon, C., Merella, M., . . . Lambert, O. (2024). A new Late Miocene beaked whale (Cetacea, Odontoceti) from the Pisco Formation, and a revised age for the fossil Ziphiidae of Peru. *Bollettino della Società Paleontologica Italiana, 63*(1), 21–43.

Blott, S. J., & Pye, K. (2001). Gradistat: A grain size distribution and statistics package for the analysis of unconsolidated sediments. *Earth Surface Processes and Landforms, 26*(11), 1237–1248. https://doi.org/10.1002/esp.261

Bosio, G., Gioncada, A., Malinverno, E., Di Celma, C., Villa, I. M., Cataldi, G., . . . Bianucci, G. (2019). Chemical and petrographic fingerprinting of volcanic ashes as a tool for high-resolution stratigraphy of the upper Miocene Pisco Formation (Peru). *Journal of the Geological Society, 176*(1), 13–28. https://doi.org/10.1144/jgs2018-071

Bosio, G., Malinverno, E., Villa, I. M., Di Celma, C., Gariboldi, K., Gioncada, A., . . . Bianucci, G. (2020a). Tephrochronology and chronostratigraphy of the Miocene Chilcatay and Pisco formations (East Pisco Basin, Peru). *Newsletters on Stratigraphy, 53*(2), 213–247. https://doi.org/10.1127/nos/2019/0525

Bosio, G., Malinverno, E., Collareta, A., Di Celma, C., Gioncada, A., Parente, M., . . . Bianucci, G. (2020b). Strontium Isotope Stratigraphy and the thermophilic fossil fauna from the middle Miocene of the East Pisco Basin (Peru). *Journal of South American Earth Sciences, 97*, 102399. https://doi.org/10.1016/j.jsames.2019.102399

Bosio, G., Gioncada, A., Di Celma, C., Villa, I. M., Pichavant, M., Urbina, M., & Bianucci, G. (2020c). Two-mica rhyolitic tephra in the East Pisco Basin (Peru): New age and dispersion constraints for the eruptions of the Eastern Cordillera of Central Andes. *Bulletin of Volcanology, 82*(6), 42. https://doi.org/10.1007/s00445-020-1373-y

Bosio, G., Collareta, A., Di Celma, C., Lambert, O., Marx, F., de Muizon, C., . . . Bianucci, G. (2021). Taphonomy of marine vertebrates of the Pisco Formation (Miocene, Peru): Insights into the origin of an outstanding Konservat-Lagerstätte. *PLoS One, 16*(7), e0254395. https://doi.org/10.1371/journal.pone.0254395

Bosio, G., Bianucci, G., Collareta, A., Landini, W., Urbina, M., & Di Celma, C. (2022). Ultrastructure, composition, and $^{87}Sr/^{86}Sr$ dating of shark teeth from lower Miocene sediments of southwestern Peru. *Journal of South American Earth Sciences, 118*, 103909. https://doi.org/10.1016/j.jsames.2022.103909

Boulila, S., Galbrun, B., Miller, K. G., Pekar, S. F., Browning, J. V., Laskar, J., & Wright, J. D. (2011). On the origin of Cenozoic and Mesozoic "third-order" eustatic sequences. *Earth-Science Reviews, 109*(3–4), 94–112. https://doi.org/10.1016/j.earscirev.2011.09.003

Bukry, D. (1981). Synthesis of silicoflagellate stratigraphy for Maastrichtian to Quaternary marine sediment. *SEPM Special Publications, 32*, 433–444.

Caffe, P. J., Trumbull, R. B., & Siebel, W. (2012). Petrology of the Coyaguayma ignimbrite, northern Puna of Argentina: Origin and evolution of a peraluminous high-SiO2 rhyolite magma. *Lithos, 134*, 179–200. https://doi.org/10.1016/j.lithos.2011.12.013

Chavez, F. P., & Messié, M. (2009). A comparison of eastern boundary upwelling ecosystems. *Progress in Oceanography, 83*(1–2), 80–96. https://doi.org/10.1016/j.pocean.2009.07.032

Coletti, G., Bosio, G., Collareta, A., Malinverno, E., Bracchi, V. A., Di Celma, C., . . . Stainbank, S. (2019). Biostratigraphic, evolutionary, and paleoenvironmental significance of the southernmost lepidocyclinids of the Pacific coast of South America (East Pisco Basin, southern Peru). *Journal of South American Earth Sciences, 96*, 102372. https://doi.org/10.1016/j.jsames.2019.102372

Collareta, A., Landini, W., Lambert, O., Post, K., Tinelli, C., Di Celma, C., . . . Bianucci, G. (2015). Piscivory in a Miocene Cetotheriidae of Peru: First record of fossilized stomach content for an extinct baleen-bearing whale. *Naturwissenschaften, 102*(11–12), 70. https://doi.org/10.1007/s00114-015-1319-y

Collareta, A., Landini, W., Chacaltana-Budiel, C., Valdivia-Vera, W., Altamirano-Sierra, A., Urbina, M., & Bianucci, G. (2017). A well preserved skeleton of the fossil shark *Cosmopolitodus hastalis* from the late Miocene of Peru, featuring fish remains as fossilized stomach contents. *Rivista Italiana di Paleontologia e Stratigrafia, 123*(1), 11–22.

Collareta, A., Lambert, O., Marx, F. G., de Muizon, C., Varas-Malca, R., Landini, W., . . . Bianucci, G. (2021a). Vertebrate Palaeoecology of the Pisco Formation (Miocene, Peru): Glimpses into the Ancient Humboldt Current Ecosystem. *Journal of Marine Science and Engineering, 9*(11), 1188. https://doi.org/10.3390/jmse9111188

Collareta, A., Di Celma, C., Bosio, G., Pierantoni, P. P., Malinverno, E., Lambert, O., . . . Bianucci, G. (2021b). Distribution and paleoenvironmental framework of middle Miocene marine vertebrates along the western side of the lower Ica Valley (East Pisco Basin, Peru). *Journal of Maps, 17*(2), 7–17. https://doi.org/10.1080/17445647.2020.1850535

DeVries, T. J. (1998). Oligocene deposition and Cenozoic sequence boundaries in the Pisco basin (Peru). *Journal of South American Earth Sciences, 11*(3), 217–231. https://doi.org/10.1016/S0895-9811(98)00014-5

DeVries, T. J., & Frassinetti, C. D. (2003). Range extensions and biogeographic implications of Chilean Neogene mollusks found in Peru. *Boletín del Museo Nacional de Historia Natural, 52*, 119–135. https://doi.org/10.54830/bmnhn.v52.2003.313

DeVries, T., & Jud, N. A. (2018). Lithofacies Patterns and Paleogeography of the Miocene Chilcatay and lower Pisco Depositional Sequences (East Pisco Basin, Peru). *Boletín de la Sociedad Geológica del Perú*, *Volumen Jubilar, 8*, 124–167.

DeVries, T. J., Urbina, M., & Judd, N. A. (2017). The Eocene-Oligocene Otuma Depositional Sequence (East Pisco Basin, Peru): Paleogeographic and Paleoceanographic Implications of New Data. *Boletín de la Sociedad Geológica del Perú, 112*, 14–38.

DeVries, T. J., Barron, J. A., Urbina-Schmitt, M., Ochoa, D., Esperante, R., & Snee, L. W. (2021). The Miocene stratigraphy of the Laberinto area (Río Ica Valley) and its bearing on the geological history of the East Pisco Basin (south-central Peru). *Journal of South American Earth Sciences, 111*, 103458. https://doi.org/10.1016/j.jsames.2021.103458

Di Celma, C., Malinverno, E., Bosio, G., Collareta, A., Gariboldi, K., Gioncada, A., . . . Bianucci, G. (2017). Sequence stratigraphy and paleontology of the upper Miocene Pisco formation along the Western side of the Lower Ica Valley (Ica desert, Peru). *Rivista Italiana di Paleontologia e Stratigrafia, 123*, 255–273.

Di Celma, C., Malinverno, E., Bosio, G., Gariboldi, K., Collareta, A., Gioncada, A., . . . Bianucci, G. (2018a). Intraformational unconformities as a record of late Miocene eustatic falls of sea level in the Pisco Formation (southern Peru). *Journal of Maps, 14*(2), 607–619. https://doi.org/10.1080/17445647.2018.1517701

Di Celma, C., Malinverno, E., Collareta, A., Bosio, G., Gariboldi, K., Lambert, O., . . . Bianucci, G. (2018b). Facies analysis, stratigraphy and marine vertebrate assemblage of the lower Miocene Chilcatay Formation at Ullujaya (Pisco basin, Peru). *Journal of Maps, 14*(2), 257–268. https://doi.org/10.1080/17445647.2018.1456490

Di Celma, C., Pierantoni, P. P., Malinverno, E., Collareta, A., Lambert, O., Landini, W., . . . Bianucci, G. (2019). Allostratigraphy and paleontology of the lower Miocene Chilcatay Formation in the Zamaca area, East Pisco basin, southern Peru. *Journal of Maps, 15*(2), 393–405. https://doi.org/10.1080/17445647.2019.1604439

Di Celma, C., Pierantoni, P. P., Volatili, T., Molli, G., Mazzoli, S., Sarti, G., . . . Bianucci, G. (2022). Towards deciphering the Cenozoic evolution of the East Pisco Basin (southern Peru). *Journal of Maps, 18*(2), 397–412. https://doi.org/10.1080/17445647.2022.2072780

Esperante, R., Brand, L. R., Chadwick, A. V., & Poma, O. (2015). Taphonomy and paleoenvironmental conditions of deposition of fossil whales in the diatomaceous sediments of the Miocene/Pliocene Pisco Formation, southern Peru – a new Fossil-Lagerstätte. *Palaeogeography, Palaeoclimatology, Palaeoecology, 417*, 337–370. https://doi.org/10.1016/j.palaeo.2014.09.029

Gariboldi, K., Gioncada, A., Bosio, G., Malinverno, E., Di Celma, C., Tinelli, C., . . . Bianucci, M. (2015). The dolomite nodules enclosing fossil marine vertebrates in the East Pisco Basin, Peru: Field and petrographic insights into the Lagerstätte formation. *Palaeogeography, Palaeoclimatology, Palaeoecology, 438*, 81–95. https://doi.org/10.1016/j.palaeo.2015.07.047

Gariboldi, K., Bosio, G., Malinverno, E., Gioncada, A., Di Celma, C., Villa, I. M., . . . Bianucci, G. (2017). Bi-

ostratigraphy, geochronology and sedimentation rates of the upper Miocene Pisco Formation at two important marine vertebrate fossil-bearing sites of southern Peru. *Newsletters on Stratigraphy, 50*(4), 417–444. https://doi.org/10.1127/nos/2017/0345

Gemeinhardt, K. (1931). Organismenformen auf der Grenze zwischen Radiolarien und Flagellaten. *Berichte der Deutschen Botanischen Gesellschaft, 49*(2), 103–110. https://doi.org/10.1111/j.1438-8677.1931.tb00388.x

Gioncada, A., Collareta, A., Gariboldi, K., Lambert, O., Di Celma, C., Bonaccorsi, E., . . . Bianucci, G. (2016). Inside baleen: Exceptional microstructure preservation in a late Miocene whale skeleton from Peru. *Geology, 44*(10), 839–842. https://doi.org/10.1130/G38216.1

Gradstein, F. M., Ogg, J. G., Schmitz, M. D., & Ogg, G. M. (2020). *Geologic Time Scale*. Amsterdam: Elsevier. https://doi.org/10.1127/nos/2020/0634

Hardenbol, J., Thierry, J., Farley, M. B., Jacquin, T., de Graciansky, P. C., & Vail, P. R. (1998). SEPM Special Publication: *Vol. 60. Mesozoic and Cenozoic sequence chronostratigraphic chart* (pp. 3–29).

Herbozo, G., Kukowski, N., Clift, P. D., Pecher, I., & Bolaños, R. (2020). Cenozoic increase in subduction erosion during plate convergence variability along the convergent margin off Trujillo, Peru. *Tectonophysics, 790*, 228557. https://doi.org/10.1016/j.tecto.2020.228557

Karstensen, J., & Ulloa, O. (2009). The Peru-Chile Current System. In J. H. Steele, K. K. Turekian, & S. A. Thorpe (Eds.), *Encyclopedia of Ocean Sciences* (pp. 385–392). Amsterdam: Elsevier. https://doi.org/10.1016/B978-012374473-9.00599-3

Kiel, S., Jakubowicz, M., Altamirano, A., Belka, Z., Dopieralska, J., Urbina, M., & Salas-Gismondi, R. (2023). The late Cenozoic evolution of the Humboldt Current System in coastal Peru: Insights from neodymium isotopes. *Gondwana Research, 116*, 104–112. https://doi.org/10.1016/j.gr.2022.12.008

Koç, N., & Scherer, R. P. (1996). Neogene Diatom Biostratigraphy of the Iceland Sea Site 907. In J. Thiede, A.M. Myhre, J. V. Firth, J. L. Johnson, & W. F. Ruddiman (Eds.), *Proceedings of the Ocean Drilling Program* (pp. 61–74). https://doi.org/10.2973/odp.proc.sr.151.108.1996

Kulm, L. D., Resig, J. M., Thornburg, T. M., & Schrader, H. J. (1982). Cenozoic structure, stratigraphy and tectonics of the central Peru forearc. In J. K. Leggett (Ed.), *Trench and forearc geology: sedimentation and tectonics on modern and ancient plate margins. Geological Society Special Publications, 10,* 151–169. https://doi.org/10.1144/GSL.SP.1982.010.01.10

Lambert, O., Bianucci, G., Post, K., de Muizon, C., Salas-Gismondi, R., Urbina, M., & Reumer, J. (2010). The giant bite of a new raptorial sperm whale from the Miocene epoch of Peru. *Nature, 466*(7302), 105–108. https://doi.org/10.1038/nature09067

Lambert, O., Collareta, A., Landini, W., Post, K., Ramassamy, B., Di Celma, C., . . . Bianucci, G. (2015). No deep diving: Evidence of predation on epipelagic fish for a stem beaked whale from the Late Miocene of Peru. *Proceedings of the Royal Society B: Biological Sciences, 282*(1815), 20151530.

Lambert, O., de Muizon, C., Malinverno, E., Di Celma, C., Urbina, M., & Bianucci, G. (2018). A new odontocete (toothed cetacean) from the Early Miocene of Peru expands the morphological disparity of extinct heterodont dolphins. *Journal of Systematic Palaeontology, 16*(12), 981–1016. https://doi.org/10.1080/14772019.2017.1359689

Lazarus, D., Barron, J., Renaudie, J., Diver, P., & Türke, A. (2014). Cenozoic Planktonic Marine Diatom Diversity and Correlation to Climate Change. *PLoS One, 9*(1), e84857. https://doi.org/10.1371/journal.pone.0084857

Locker, S., & Martini, E. (1986). Silicoflagellates and some sponge spicules from the southwest Pacific, Deep Sea Drilling Project, Leg 90. *Initial Reports of the Deep Sea Drilling Project, 90*, 887–924. https://doi.org/10.2973/dsdp.proc.90.116.1986

Malinverno, E., Bosio, G., Di Celma, C., Gariboldi, K., Gioncada, A., Pierantoni, P. P., . . . Bianucci, G. (2021). (Bio)stratigraphic overview and paleoclimatic-paleoceanographic implications of the middle-upper Eocene deposits from the Ica River Valley (East Pisco Basin, Peru). *Palaeogeography, Palaeoclimatology, Palaeoecology, 578*, 110567. https://doi.org/10.1016/j.palaeo.2021.110567

Marty, R., Dunbar, R., Martin, J. B., & Baker, P. (1988). Late Eocene diatomite from the Peruvian coastal desert, coastal upwelling in the eastern Pacific, and Pacific circulation before the terminal Eocene event. *Geology, 16*(9), 818–822. https://doi.org/10.1130/0091-7613(1988)0162.3.CO;2

Maruyama, T., & Shiono, M. (2003). Middle Miocene to Pleistocene diatom biostratigraphy of the northwest Pacific at Sites 1150 and 1151. *Proceedings of the Ocean Drilling Program, Scientific Results, 186*, 1–38.

Mertz, D. (1966). Mikropaläontologische un sedimentologische untersuchung der Pisco-Formation Südperus. *Palaeontographica. Abteilung B, Paläophytologie, 118*(1–3), 1–51.

Miller, K. G., Wright, J. D., & Fairbanks, R. G. (1991). Unlocking the Ice House: Oligocene-Miocene oxygene isotopes, eustasy, and margin erosion. *Journal of Geophysical Research, 96*(B4), 6829–6848. https://doi.org/10.1029/90JB02015

Miller, K. G., Mountain, G. S., Browning, J. V., Kominz, M., Sugarman, P. J., Christie-Blick, N., . . . Wright, J. D. (1998). Cenozoic global sea level, sequences, and the New Jerseytransect: Results from coastal plain and continental slopedrilling. *Reviews of Geophysics, 36*(4), 569–601. https://doi.org/10.1029/98RG01624

Penven, P., Echevin, V., Pasapera, J., Colas, F., & Tam, J. (2005). Average circulation, seasonal cycle, and mesoscale dynamics of the Peru Current System: A modeling approach. *Journal of Geophysical Research. Oceans, 110*(C10), C10021.

Perch-Nielsen, K. (1985a). Silicoflagellates. In H. M. Bolli, J. B. Saunders, & K. Perch-Nielsen (Eds.), *Plankton*

Stratigraphy (pp. 811–846). Cambridge: University Press.

Perch-Nielsen, K. (1985b). Cenozoic calcareous nannofossils. In H. M. Bolli, J. B. Saunders, & K. Perch-Nielsen (Eds.), *Plankton Stratigraphy* (pp. 427–554). Cambridge: University Press.

Piperno, D. R. (2006). *Phytoliths: a comprehensive guide for Archaeologists and Paleoecologists*. New York: AltaMira Press.

Romero, D., Valencia, K., Alarcón, P., Peña, D., & Ramos, V. A. (2013). The offshore basement of Perú: Evidence for different igneous and metamorphic domains in the forearc. *Journal of South American Earth Sciences, 42*, 47–60. https://doi.org/10.1016/j.jsames.2012.11.003

Scherer, R. P., Gladenkov, A. Y., & Barron, J. A. (2007). Methods and applications of Cenozoic marine diatom biostratigraphy. *Paleontological Society Papers, 13*, 61–83. https://doi.org/10.1017/S1089332600001467

Thornburg, T., & Kulm, L. D. (1981). Sedimentary basins of the Peru continental margin: Structure, stratigraphy and Cenozoic tectonics from 6° to 16° S latitude. *Geological Society of America, 154*, 393–422. https://doi.org/10.1130/MEM154-p393

Villa, I. M., & Bosio, G. (2023). "Excess Ar" by laboratory alteration of biotite. *Geology, 51*(1), 121–125. https://doi.org/10.1130/G50503.1

Viveen, W., & Schlunegger, F. (2018). Prolonged extension and subsidence of the Peruvian forearc during the Cenozoic. *Tectonophysics, 730*, 48–62. https://doi.org/10.1016/j.tecto.2018.02.018

Von Huene, R., & Suess, E. (1988). Ocean Drilling Program Leg 112, Peru continental margin: Part 1, tectonic history. *Geology, 16*(10), 934–938. https://doi.org/10.1130/0091-7613(1988)0162.3.CO;2

Westerhold, T., Marwan, N., Drury, A. J., Liebrand, D., Agnini, C., Anagnostou, E., . . . Zachos, J. C. (2020). An astronomically dated record of Earth's climate and its predictability over the last 66 million years. *Science, 369*(6509), 1383–1387. https://doi.org/10.1126/science.aba6853

White, J. D. L., & Houghton, B. F. (2006). Primary volcaniclastic rocks. *Geology, 34*(8), 677–680. https://doi.org/10.1130/G22346.1

Yanagisawa, Y., & Akiba, F. (1990). Taxonomy and phylogeny of the three marine diatom genera, *Crucidenticula, Denticulopsis* and *Neodenticula. Bulletin of the Geological Survey of Japan, 41*(5), 197–301.

Manuscript received: 12.08.2024
Revisions requested: 30.08.2024
Revised version received: 21.10.2024
Accepted: 10.11.2024

The pdf version of this paper includes an electronic supplement

Please save the electronic supplement contained in this pdf-file by clicking the blue frame above. After saving rename the file extension to .zip (for security reasons Adobe does not allow to embed .exe, .zip, .rar etc. files).

Table of contents – Electronic Supplementary Material (ESM)